Towards the Transition State Structure of AlkA-Catalyzed *N*-Glycoside Hydrolysis using Kinetic Isotope Effects

By
Amanda A. Ramnarine, B. Sc.

A Thesis
Submitted to the School of Graduate Studies
in Partial Fulfillment of the Requirements
for the Degree
Master of Science

McMaster University

MASTER OF SCIENCE (2008) McMaster University

(Biochemistry and Biomedical Sciences) Hamilton, Ontario

TITLE: Toward the Transition State Structure of AlkA-Catalyzed *N*-Glycoside Hydrolysis using Kinetic Isotope Effects

AUTHOR: Amanda A. Ramnarine, B. Sc. (McMaster University)

SUPERVISOR: Dr. Paul J. Berti

NUMBER OF PAGES: x, 69

ABSTRACT

AlkA is a monofunctional DNA glycosylase from *E.coli.* This enzyme catalyzes the hydrolysis of the *N*-glycosidic bond, initiating the first step in the base excision repair pathway. This activity is crucial to the maintenance of the genetic code, as the persistence of DNA aberrations can have significant cellular consequences including mutation, and inhibition of DNA replication and transcription. This enzyme has a broad substrate specificity catalyzing the excision of various lesions (including alkylation, oxidation and deamination products) from DNA. While biochemical and structural studies have been carried out on AlkA; how this enzyme is able to recognize and excise a variety of structurally diverse lesions from DNA and the mechanism by which this excision occurs remains unknown. In this study we have shown that a stem-loop DNA structure containing a hypoxanthine bulge is an optimal substrate for TS analysis of AlkA-catalyzed *N*-glycoside hydrolysis. In addition, we have developed methods to synthesize radiolabeled deoxyinosine triphosphate (dITP) and incorporate this radiolabeled nucleotide into the stem-loop DNA structure. We have developed a facile method of purification for his-tagged AlkA and his-tagged AlkA containing a TEV protease recognition site (for removal of the his-tag), and have shown that these proteins display an activity similar to that of wild-type AlkA. The [1'-^{3}H] KIE was measured using liquid scintillation in a proof-of-principle experiment. The observed value of 1.046 is indicative of either a relatively synchronous A_ND_N (S_N2) TS or an early $D_N{*}A_N$ (S_N1) TS with oxacarbenium ion character in the sugar ring, but significant bond order to the leaving group base still remaining. Future work involves repeat measurements of the [1'-^{3}H] KIE to validate the accuracy of the measurement observed here, examination of

commitment to catalysis and optimization of the hypoxanthine bulge substrate synthesis. Analysis of KIEs at additional sites on the hypoxanthine base and sugar ring will contribute to TS analysis of AlkA-catalyzed *N*-glycoside hydrolysis and help elucidate the mechanism of hydrolysis.

ACKNOWLEDGMENTS

I would like to thank my supervisor Dr. Paul Berti, for giving me the opportunity to work in his lab as an undergraduate and graduate student, and for the support and guidance that he has provided me with throughout this project. I would also like to thank my committee members Dr. Murray Junop and Dr. Guiseppe Melacini, whose feedback and advice have been an invaluable resource to me. I would like to thank Dr. Pat O'Brien for the kind gift of wild type AlkA protein as well as plasmids containing histidine-tagged variants of alkA. I would also like to thank Dr. Joe A.B. McCann, whose work on the kinetic isotope effects of the MutY reaction laid the groundwork for the AlkA study.

I would like to thank the past and present members of the Berti lab for their support and encouragement. To Meghann Clark, Grace Lou, Jen Baker, Eddie Morrison, Kate MacKeracher, Paul Chindemi, Dr. Mohamed Changalov and Dr. Paul Loncke, you have made my time at McMaster University a wonderful experience.

I would finally like to thank my brothers Ray and Neil, my parents, and my dear friends Kenrick, Tammy and Diana for all of their inspiration and encouragement.

TABLE OF CONTENTS

LIST OF ABBREVIATIONS

AAG- Human 3-methyladenine DNA Glycosylase II;

ABESF- 4-(2-aminoethyl) benzenesulphonyl fluoride hydrochloride;

AlkA - *Escherichia coli* 3-methlyadenine DNA Glycosylase II;

ATI26- 26 base stem-loop substrate for KIE studies of the AlkA reaction;

BER- Base Excision Repair;

dATP- Deoxyadenosine triphosphate;

dITP- Deoxyinosine triphosphate;

hAPE1- Human Apurinic/Apyrimidinic Endonuclease I;

hOOG1- Human 8-Oxoguanine DNA Glycosylase;

HhH- Helix-hairpin-Helix;

IPTG - Isopropyl-beta-D-thiogalactopyranoside;

KIE- Kinetic Isotope Effect;

MMLV- Moloney Murine Leukemia Virus;

MS- Mass Spectrometry

MTAN- 5'-Methylthioadenosine Nucleosidases;

MutY- *Escherichia coli* Adenine DNA Glycosylase;

PNP- Purine Nucleoside Phosphorylase;

TEV- Tobacco Etch Virus;

TS- Transition State;

LIST OF FIGURES

1.0 INTRODUCTION

1.1 DNA Damage

Assault to the genome can occur a number of ways, and if left unrepaired the cellular consequences include mutation and inhibition of replication and transcription, leading to cell senescence or apoptosis (*1, 2*). The most common forms of DNA damage include oxidation, alkylation, and deamination (*3, 4*).

Oxidative damage results from the formation of reactive oxygen species (ROS). ROS can arise in the cell by exposure to exogenous agents such as redox chemicals and ionizing radiation, or as a result of normal aerobic cellular processes (*5*). These species can generate a variety of lesions such as thymine glycol, 5-formyluracil, 4,6-diamino-5-formamidopyrimidine and 8-oxoguanine. Such lesions can block replication (thymine glycol) or stimulate mutation (8-oxoguanine). Oxidative stress can also lead to the formation of DNA double stranded breaks and DNA-protein cross-links (*6*).

Alkylative damage can arise as a result of exposure to environmental alkylating agents or endogenous species such as S-adenosylmethionine (SAM). These agents can attack the heterocyclic atoms of the bases as well as the phosphodiester backbone. Alkylating (or methylating) agents can be classified as S_N1 or S_N2 agents, depending on the mechanism of alkylation (methylation). *N*-methyl-*N*-nitrosourea (MNU) and *N*-methyl-*N*-nitro-*N*-nitrosoguanidine (MNNG) for example, are S_N1 methylating agents, while methylmethane sulphonate (MMS) and methyl halides are S_N2 methylating agents (*7*). The most common form of alkylation damage is 7-methylguanine (7MeG). This lesion is generated by the S_N1 agent MNU as well as the S_N2 agent MMS, and constitutes approximately 70-80% of all DNA alkylation damage. The second most

abundant lesion 3-methyladenine (3MeA) (which accounts for 10-15% of all DNA alkylation damage) is highly damaging acting as a block to DNA replication (*3, 8*).

Deamination can occur spontaneously in the cell (albeit slowly), via hydrolytic deamination of the amino groups on purines and pyrimidines (*3*). This process can also result from exposure to reactive species such as nitrous acid (HNO_2) and nitric oxide (NO) (*9, 10*) as well as ionizing radiation and UV light (*11*), or as a result of the action of deaminases. Deamination of adenine, guanine and cytosine can result in the presence of hypoxanthine, xanthine (and/or oxanthine) and uracil in DNA, respectively. The persistence of these lesions in DNA can lead to mutations. For example, hypoxanthine has base pairing properties similar to guanine, and can thus trigger AT to GC transition mutations (*9, 12*). Interestingly, NO is overproduced by macrophages during bacterial infection and inflammation. This overproduction in chronically inflamed tissues has been associated with carcinogenesis (*10, 13, 14*).

DNA damage or abnormalities in DNA damage repair have been associated with neurodegenerative disorders such as Alzheimer's disease as well as cancer (*3, 5, 6, 15*). It is imperative to understand 1) how DNA damage is induced, 2) the mechanisms by which this damage is repaired, 3) how a deficiency in repair contributes to disease, and 4) how these repair pathways can provide a basis for the design of therapeutic strategies.

1.2 DNA Repair

Organisms have evolved complex pathways to correct DNA damage and maintain genetic integrity. These pathways involve both damage recognition and repair. A number of repair mechanisms exist including direct reversal, mismatch repair (MMR), nucleotide excision repair (NER) and base excision repair (BER). Direct reversal is

common in the repair of some alkylative lesions (*16*). Direct reversal mechanisms are involved in the repair of single base lesions and occur through the enzymatic removal of the chemical modification to regenerate the undamaged base. In some cases this type of repair results in inactivation of the repair enzyme. MMR is responsible for the repair of DNA mismatches and deletion/insertion loops that may develop during DNA replication, as well as mismatches that may arise as a result of damaged bases (*17*). This type of repair involves a multi-protein complex which recognizes and initiates removal of the mismatch. MMR entails the removal and replacement of an oligonucleotide patch containing the mismatched base (long patch repair). The NER pathway is responsible for the repair of lesions that cause significant distortion to the double helix, such as larger bulky adducts, strand breaks and DNA-protein cross-links (*18, 19*). This mechanism of repair also employs a complex of proteins to initiate and carry out long patch repair. The most common repair mechanism for small single base damage is the BER pathway. This pathway is involved in the repair of oxidative and alkylative lesions, as well as deamination products. The BER pathway is conserved across a diversity of organisms, suggesting evolutionary importance.

1.3 The BER Pathway

There are two types BER pathways; short patch and long patch repair (Figure 1.1). Short patch repair involves the replacement of the single damaged nucleotide, while long patch repair involves the replacement of the damaged nucleotide as well as several nucleotides downstream of the damaged site. Long patch repair employs the activity of an (additional) endonuclease, FEN1, which removes the 5' single stranded overhang generated by this type of repair (*4*).

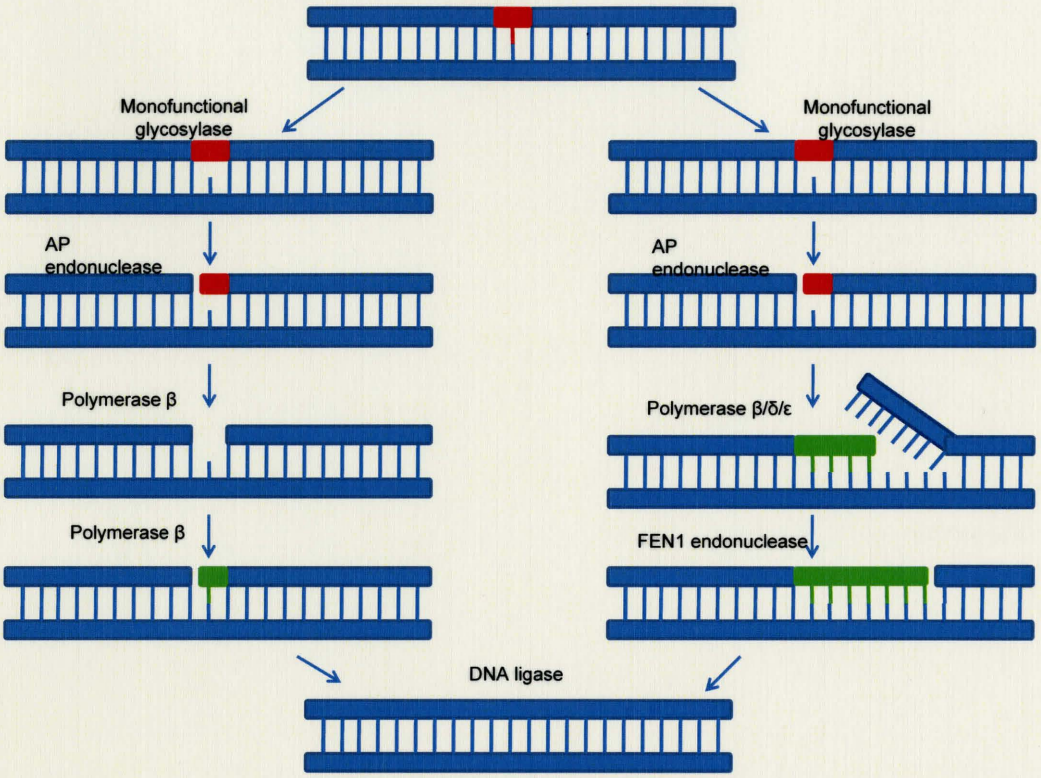

Figure 1.1. Short-patch vs. Long-patch Repair

The first step in the pathway is carried out by a monofunctional or bifunctional DNA glycosylase. These enzymes are able to identify damaged bases and catalyze the cleavage of the *N*-glycosidic bond, releasing the damaged base and generating an abasic site (Figure 1.2). Monofunctional DNA glycosylases initiate BER using a water molecule for nucleophilic attack at the anomeric carbon. The action of an abasic endonuclease subsequently cleaves the phosphodiester bond 5' to the abasic site, generating a 5' phosphate abasic nucleotide and a 3' hydroxyl. Next, the lyase action of a DNA repair polymerase (pol β in humans) carries out a β-elimination reaction, cleaving the phosphodiester bond 3' to the abasic nucleotide (*4, 20*). The polymerase can then incorporate the correct nucleotide into the DNA strand, and the repair process is

completed by a DNA ligase that seals the nick between the 3' hydroxyl of the inserted nucleotide and the 5' phosphate of the adjacent nucleotide. Conversely, bifunctional DNA glycosylases use an active site amine to attack at the anomeric carbon, displacing the damaged base and generating a covalent Schiff base intermediate. This intermediate subsequently triggers a β-elimination reaction 3' to the abasic site. The action of a 3'phoshphodiesterase removes the abasic nucleotide and the resulting gap is filled in by a replicative polymerase and sealed by a DNA ligase (*4*).

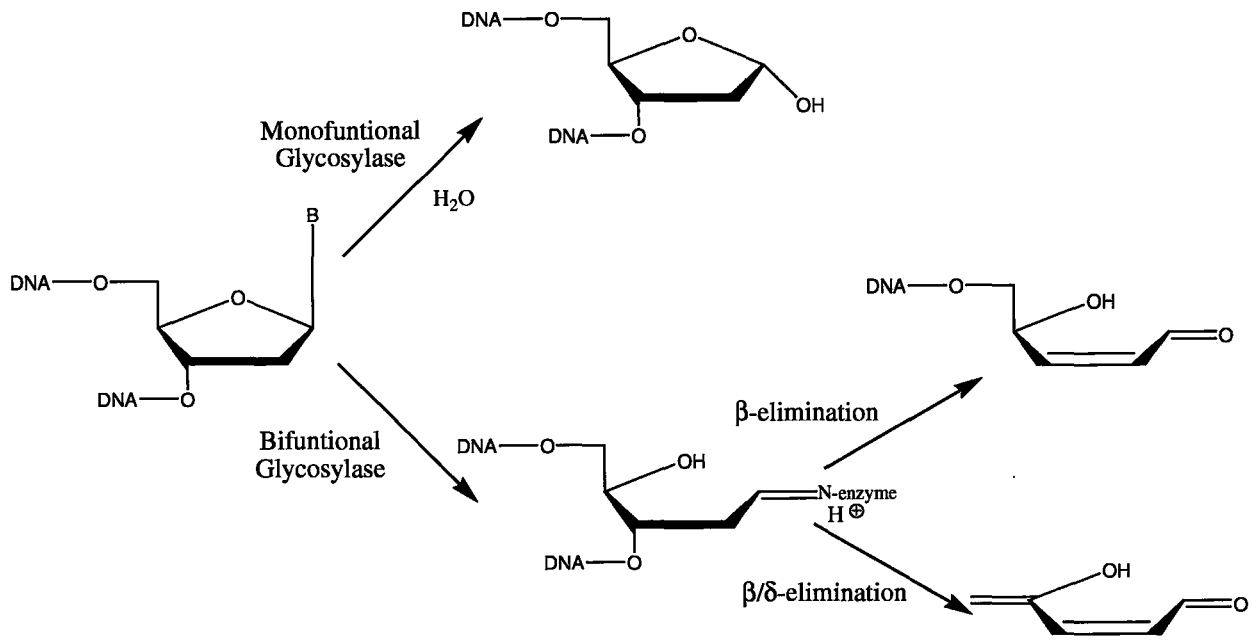

Figure 1.2. Monofunctional vs. Bifunctional DNA glycosylases.

1.4 DNA Glycosylases

The role of the DNA glycosylase is crucial to the repair process. Not only do these enzymes scan DNA and identify damaged bases amongst an excess of normal nucleotides, but cleavage of the *N*-glycosidic bond initiates the process of repair. A number of different DNA glycosylases exist, recognizing and removing different lesions from DNA. Many of these glycosylases have a narrow substrate specificity. Uracil DNA

glycosylase (UDG), for example, is capable of removing only uracil from DNA. However some DNA glycosylases, such as 3-methyladenine DNA glycosylase II (AlkA) and its functional counterpart in mammals AAG, have a broad substrate specificity (*4, 21-23*).

1.5 Mechanisms of N-Glycoside Hydrolysis

DNA glycosylases initiate the BER pathway by removing the damaged base, via hydrolysis of the N-glycosidic bond, a nucleophilic substitution. Nucleophilic substitution reactions stereotypically occur through S_N2 (A_ND_N) or S_N1 (D_N*A_N) mechanisms. In an S_N2 (A_ND_N) reaction, nucleophilic attack at the anomeric carbon occurs simultaneously with dissociation of the leaving group. A_N represents nucleophilic attack and D_N indicates nucleophilic dissociation in IUPAC nomenclature (*24*) (Figure 1.3).

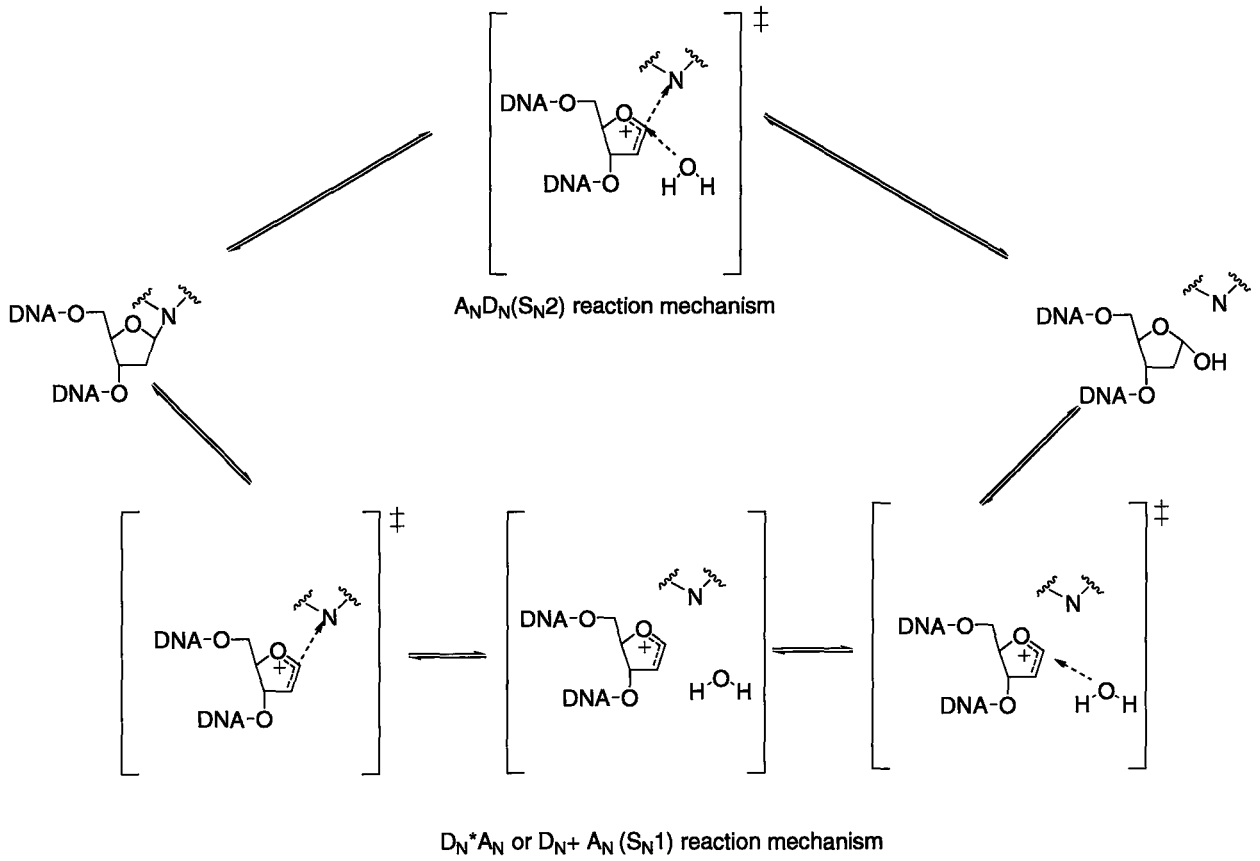

Figure 1.3. A_ND_N and $D_N{*}A_N$ or $D_N{+}A_N$ pathways.

This type of concerted reaction pathway has a single transition state which can be further categorized as associative or dissociative depending on the amount of bond order present at the TS. An associative S_N2 transition state retains significant bond order to the leaving group at the TS, with the sum of the bond orders to the nucleophile and leaving groups □ 1. A dissociative S_N2 transition state demonstrates minimal bond order to the leaving group at the TS (Figure 1.4), with the sum of the bond orders to the nucleophile and leaving group □ 1.

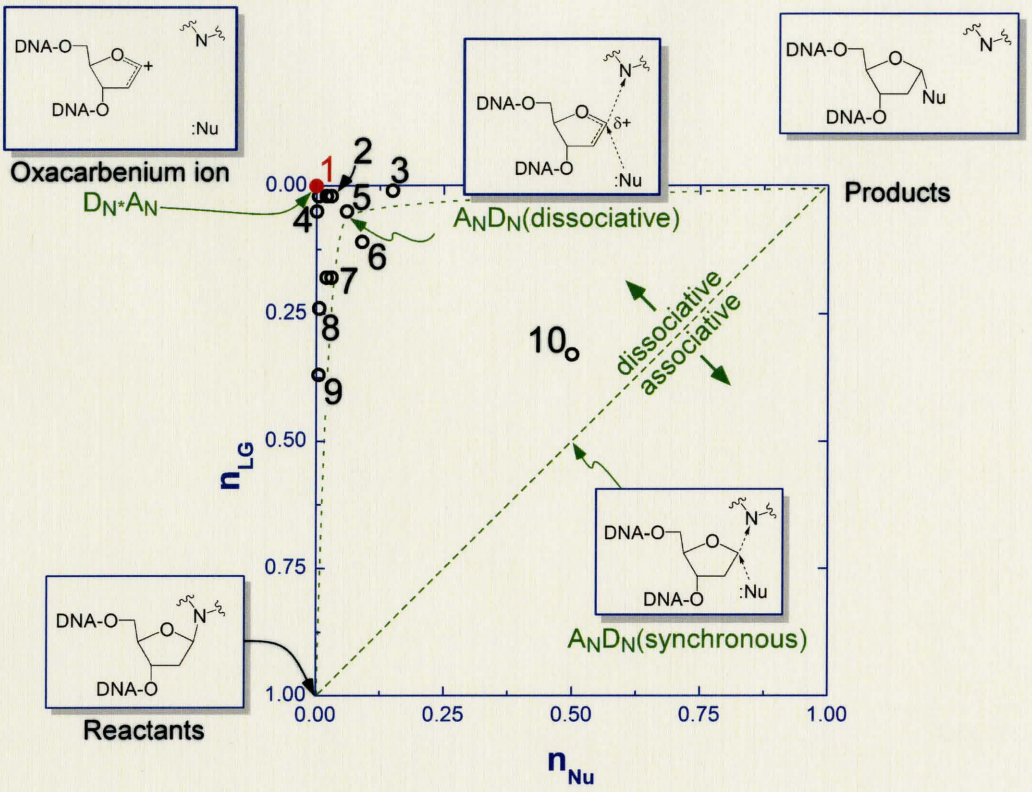

Figure 1.4. Reaction space for N-glycoside hydrolysis. (nNu) represents the bond order from C1' to the nucleophile and (nLG) represents the bond order from C1' to the leaving group. The numbers represent the experimental TSs for various enzymes including the D_N*A_N TS of ricin and the A_ND_N TS of chlorea toxin hydrolysis (22).

The reaction can also employ an S_N1 (stepwise) mechanism involving departure of the leaving group prior to nucleophilic association, and the existence of a discrete oxacarbenium ion intermediate. This mechanism consists of two transition states; one for leaving group dissociation, and the second for nucleophilic addition. This type of reaction mechanism is referred to as $D_N + A_N$ or D_N*A_N depending on the status of the oxacarbenium intermediate. A $D_N + A_N$ mechanism is distinguished by the leaving group base and oxacarbenium intermediate diffusionally separating before nucleophilic

addition. In a D_N*A_N reaction the oxacarbenium ion intermediate does not exist long enough for the leaving group to diffusionally separate (*4, 22*).

1.6 Enzyme of Interest – AlkA and the HhH Superfamily

AlkA is capable of excising several oxidative and alkylative lesions, as well as some deamination products and alkyl adducts. This enzyme's ability to remove a number of structurally diverse lesions from DNA presents intriguing questions about its mechanism of base excision.

AlkA is a member of the helix-hairpin-helix (HhH) superfamily of BER proteins, which also includes MutY (*25, 26*). Structural and sequence comparisons between DNA glycosylases of this family have revealed a few commonalities. These include the conserved HhH motif, a conserved aspartic acid residue within the active site, and a nucleotide flipping mechanism thought to facilitate the extraction and insertion of a damaged base from the double helix and into the enzyme's active site.

1.7 The Helix-Hairpin-Helix Motif

The HhH motif is one of a small subset of structural motifs that are involved in DNA binding. This motif is characterized by two antiparallel α-helices linked by a small hairpin-like loop that interacts with the DNA. The HhH motif is responsible for non-sequence specific protein binding to DNA and is commonly found in DNA polymerases and DNA repair enzymes (*2, 27*). This motif is thought to anchor DNA to the protein and facilitate DNA bending and base flipping.

1.8 Base Extrusion

A characteristic feature of most DNA glycosylases is their ability to facilitate the extraction of abnormal lesions from a vast excess of undamaged bases. These enzymes utilize a base flipping mechanism to gain access to aberrant bases buried within the double helix. There are three types of enzyme-induced base flipping; these include flipping of the lesion itself, flipping of the base paired to the lesion, and flipping of both the lesion and its base pair (*4*). Enzymatic base flipping is generally accompanied by distortion of the DNA at the damaged site. This DNA bending has a two-fold effect on base pair opening and subsequent base flipping. Bending reduces the energy the enzyme must exert in order to overcome base stacking interactions, while simultaneously generating backbone strain that can be relieved by base pair opening (*28*). DNA glycosylases such as MutY and UDG exhibit this type of active base flipping. It has also been suggested that damaged nucleotides are more susceptible to base flipping as a result of poor base stacking and increased flexibility of DNA lesions (Figure 1.5). This susceptibility to distortion may facilitate damage recognition by the enzyme (*29-31*). For example, the base flipping equilibrium constant for an unstable base pair, resulting from abnormal pairing with a damaged nucleotide, is higher than that of a normal Watson-Crick base pair (*22*).

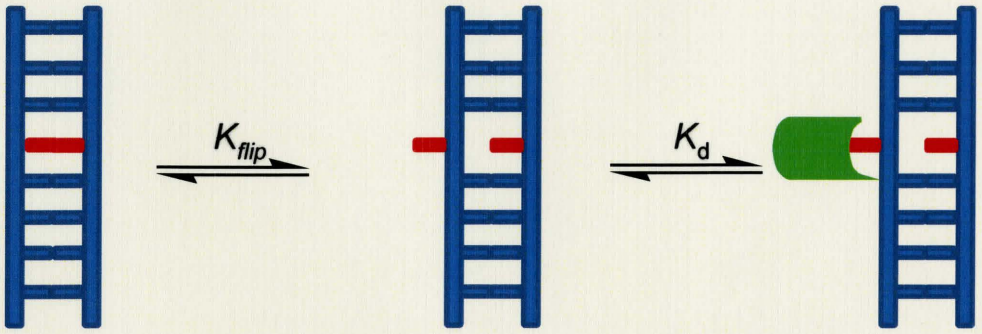

Figure 1.5. Spontaneous base flipping of damaged bases. AlkA (green) uses the higher K_{flip} of unstable base pairs to recognize damaged bases.

Consequently it has been proposed that certain DNA glycosylases such as AlkA, trap extrahelical bases that form spontaneously in DNA (*32, 33*). Some DNA glycosylases use a "wedge" group amino acid to facilitate bending and base flipping (Figure 1.6). This wedge group provides steric bulk to circumvent reinsertion of the damaged base, while helping to push the lesion from the duplex, as the enzyme attaches to and distorts the DNA (*4*).

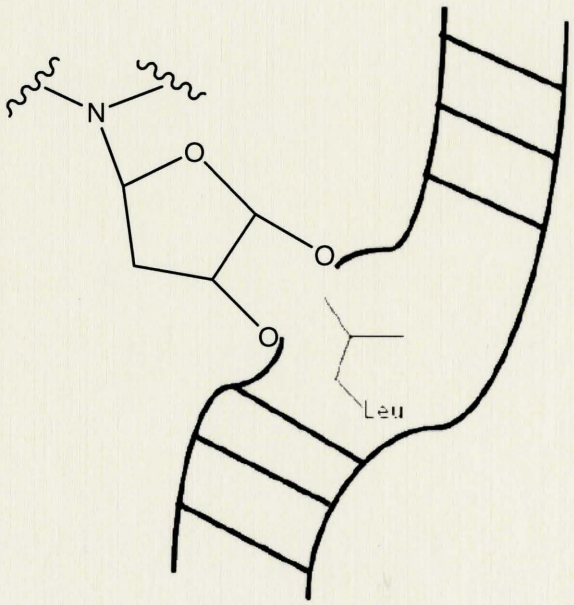

Figure 1.6. The "wedge" group amino acid (shown here as a Leucine for enzymes such as UDG and AlkA) helps to push the damaged base from the duplex and prevent re-insertion.

1.9 The Conserved Aspartic Acid

The role of the invariant Asp residue in this superfamily of enzymes remains unclear. Mutations of this conserved residue to Asn in AlkA, MIG (*34*), MutY (*25, 35*) and hOGG1(*36*) result in dramatic decreases in enzyme activity, suggesting catalytic importance. However, a mutation of the conserved Asp to Ala in MIG, showed only a moderate 16-fold decline in activity (*34*). In addition, Asp mutations to Glu and Gln in hOGG1 decreased the protein's melting temperature, but these mutants showed near wild-type activity (*36*). This residue may have more of a structural role, as suggested by helix-capping hydrogen bonds the conserved Asp makes at the N-terminus of an α-helix in all HhH enzymes (*34*). These hydrogen bonds restrict the residue's ability to interact with the substrate base, arguing against a direct role in catalysis (*22*). Thus, it is not conclusive whether this conserved Asp is catalytically relevant, or if a mutation to Asn introduces interactions within the active site that are not favourable to N-glycoside hydrolysis.

1.10 Function of AlkA

In *E.coli*, AlkA is expressed at basal levels; however exposure to methylating agents induces an adaptive response, up-regulating AlkA expression as well as three other proteins, Ada, AidB and AlkB (Figure 1.7) (*7, 37*). Ada is a multifunctional protein, in which the N-terminal domain carries out the repair of S_p-methylphosphotriester, while the C-terminal domain is able to directly repair alkylated guanine. Repair of S_p-methylphosphotriester alkylates the N-terminal domain, transforming it into a potent transcriptional activator and inducing the Ada Response. While both AidB and AlkB are proposed to be involved in direct repair of alkylation

damage, AlkA is responsible for N-glycoside bond hydrolysis, releasing the damaged base from DNA. It catalyzes the first step of the BER pathway (*7, 16, 37*).

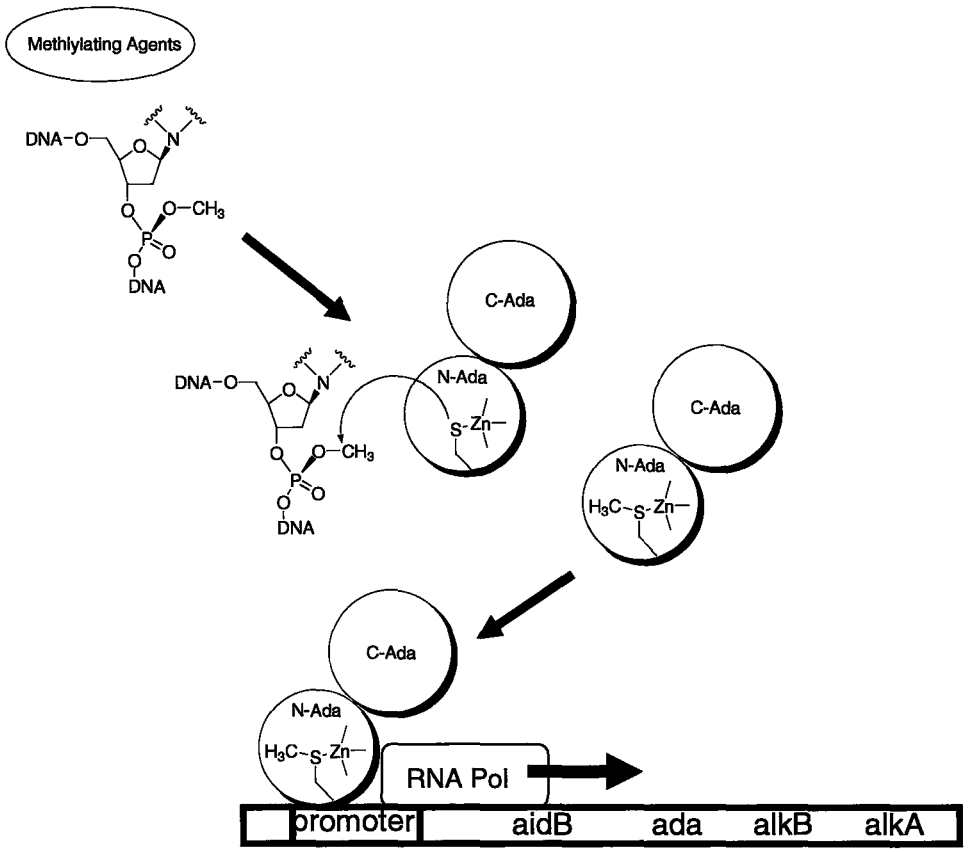

Figure 1.7. The Adaptive Response. Repair of the phosphodiester backbone is triggered by N-Ada, which is then converted into a transcriptional activator, upregulating AlkA expression.

1.11 Structure of AlkA

AlkA is a globular protein comprised of three domains. The N-terminal of the protein consists of 88 amino acids which fold into a 5-stranded antiparallel β sheet and two α-helices. The presence of this α-β sandwich motif in domain 1 is interesting, as it is also found in the TATA box-binding protein (TBBP). It has been postulated that the

solvent-exposed face of the β-sheet, which contains aromatic and hydrophobic interactions, maybe involved in DNA minor groove interactions, similar to TBBP (*38, 39*). However, the biological function of this domain remains unknown. The second domain of the glycosylase is made up of six α-helices, which form a 6-helical bundle. This domain contains the hallmark helix-hairpin-helix (HhH) motif of the HhH superfamily of DNA binding proteins. It is situated adjacent to a deep pocket that lies between domain 2 and domain 3 of the protein. This cleft constitutes the active site of the enzyme, and is lined with aromatic amino acids. The active site also contains the conserved aspartic acid residue (Asp 238). Domain 3 of AlkA consists of 4 α-helices (*38, 39*).

AlkA crystals showed cracking when soaked with methylated substrates, suggesting movement in the walls comprising the active site. This movement suggests that the aromatic active site is flexible and is reflect by the enzyme's broad substrate specificity. It is speculated that these aromatic residues, such as Trp272 and Tyr222, interact with extrahelical nucleosides via π donor-acceptor interactions.

1.12 Oxacarbenium Ion Stabilization vs. Base Catalyst --- The role of Aspartic Acid 238

X-ray crystal structures of bacterial and human 3-methyladenine DNA glycosylases in complex with an assortment of DNA substrates, as well as nucleoside hydrolyases have posed a number of questions regarding AlkA's mechanism of *N*-glycoside hydrolysis and the potential role of Asp238.

The human 3-methyladenine DNA glycosylase (AAG), while not a member of the HhH superfamily of proteins, demonstrates a broad substrate specificity similar to AlkA (*40*). AAG was crystallized in complexes with DNA containing pyrollidine or 1-N^6-ethenoadenine (*40-42*). These structures revealed a water molecule in the active site, positioned between Glu125 and the back of an extrahelical nucleoside, suggesting that Glu125 functions as a base catalyst and also providing evidence for an S_N2 reaction mechanism (*41*). In the case of AlkA, Asp238 could take on this potential role of general base catalyst. This role of base catalyst was also supported by the bell-shaped pH profile observed for AlkA catalyzed excision of guanine and 1-N^6-ethenoadenine substrates. The observed pK_a's of 6.0 and 6.9 are suggestive of general acid/base catalysis, where active site residues Tyr273 and Tyr222 have been proposed to act as an acid catalyst and the conserved Asp238 has been proposed as a base catalyst (*22*). Crystal structures of some nucleoside hydrolyases (NH's) involved in purine salvage pathways, NH IU (*43, 44*) and NH IAG (*45*), as well as MTA nucleosidase (*46*) (involved in methionine recycling) also implicate the role of a base catalyst. These structures reveal an Asp or Glu residue positioned below the plane of the substrate's ribosyl ring within the active site. In such instances, it has been suggested that these residues are not electrostatically stabilizing an oxacarbenium ion intermediate; rather, they are functioning as a general base to activate a nucleophile (*22, 47*).

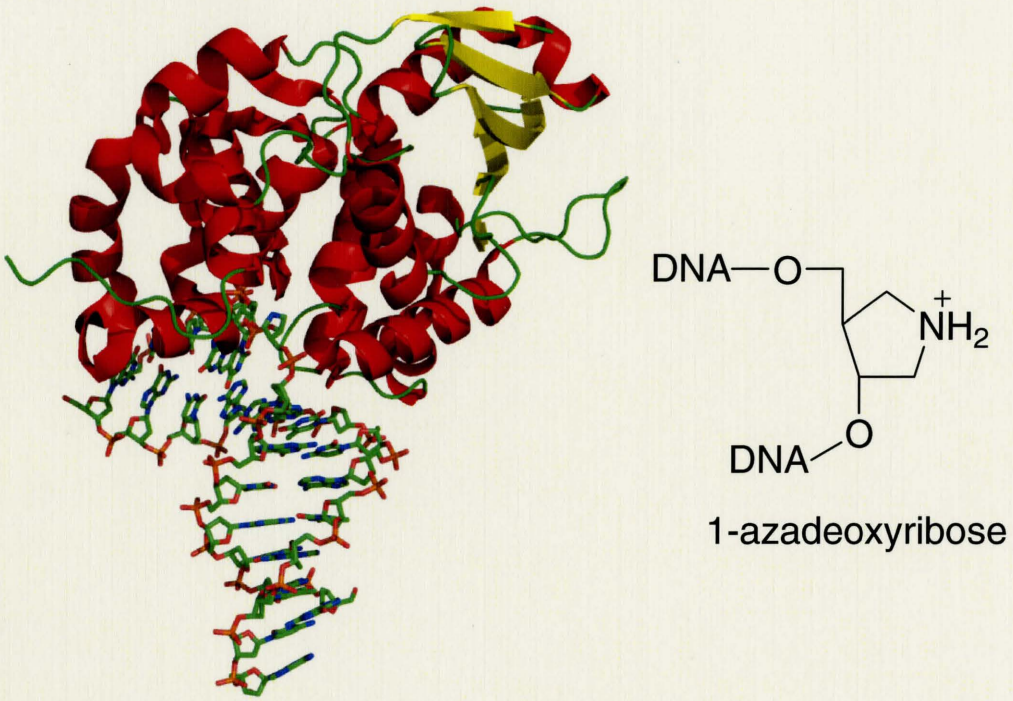

Figure 1.8. An X-ray crystal structure of AlkA in complex with the transition state mimic 1-aza-deoxyribose.

AlkA was crystallized in complex with an abasic transition state (TS) mimic, 1-azaribose (Figure 1.8) (*1*). Hollis et al., proposed that the close proximity of the positively charged N1 (which corresponds to C1 of a 3-methyladenine substrate) to Asp238 (3.1Å), indicates that Asp238 may directly stabilize an oxacarbenium intermediate through electrostatic interactions, and proposed a D_N*A_N (S_N1) reaction mechanism (in which leaving group dissociation and nucleophilic attack occur on the same face of the carbocation) for N-glycoside hydrolysis (*42*). It was noted previously, that AlkA crystals showed signs of cracking when soaked with methylated substrates. This cracking was attributed to movement in domains 2 and 3. This motion may be necessary for substrate binding and may create an opportunity for water to bind AlkA as

well (*22*). The role of Asp238 in oxacarbenium ion stabilization was further supported by the low K_d values of two oxacarbenium ion mimics 1-aza-deoxyribose and 4-aza-deoxyribose (paired with cytosine), which were 100 pM and 16 pM respectively (*21, 22, 38*).

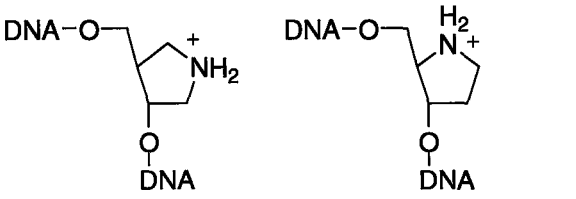

1-azadeoxyribose 4-azadeoxyribose

1.13 Substrate Specificity of AlkA

AlkA's broad substrate specificity raises questions regarding the enzyme's mechanism of N-glycoside hydrolysis. Alkylated purines bearing a positive charge such as 3-methyladenine (3meA) and 7-methylguanine (7meG) are able to form strong π-donor/π-acceptor interactions with the aromatic amino acids of the active site. This allows the enzyme to stabilize the damaged base in the extrahelical position while the *N*-glycosidic bond is cleaved. The positive charge on the damaged base makes the purine ring electron withdrawing. This destabilizes the glycosidic bond, resulting in a reduced activation energy barrier and efficient excision by AlkA. Strong interactions between aromatic active site residues and the cationic base, in addition to the inherently weakened glycosidic bond, make this type of substrate favourable (*4*). However, AlkA is also capable of removing neutral deamination products including xanthine and hypoxanthine (Hx), as well as neutral alkyl adducts such as 1,N^6-ethenoadenine (*21*). While π-π stacking interactions between these neutral lesions and aromatic residues lead to

favourable binding within the active site, they are removed at much lower rates than methylated purines (*4*). For example, the single turnover rate constant for excision of 7meG (paired with C) is 1.2 min^{-1}, while it is 2.9×10^{-2} min^{-1} for Hx (paired with C) (*21*). Investigations into AlkA substrate specificity by O'Brien et al., suggest that positively charged purine bases such as 7meG are subject to a similar amount of catalysis by the enzyme, as neutral lesions such as hypoxanthine. However because positively charged purines are intrinsically less stable than neutral lesions, their excision rates are higher.

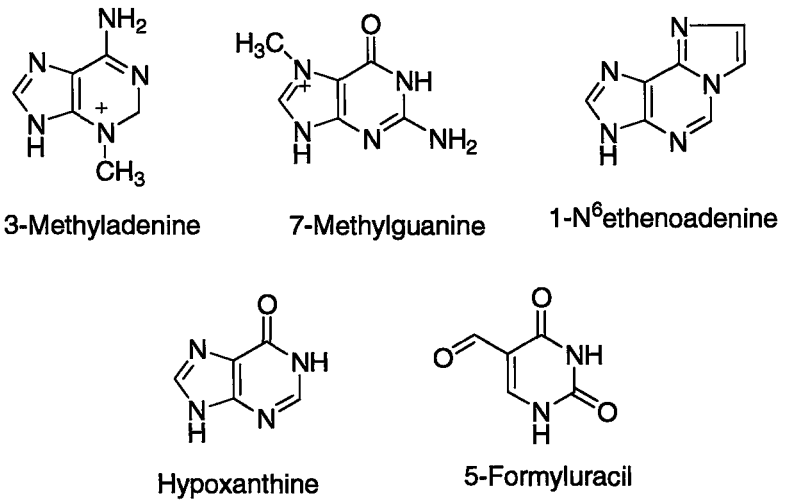

Figure 1.9. Substrates of AlkA. AlkA is capable of excising various alkylation, oxidation and deaminative lesions.

Analysis of rate enhancements (rate enhancement = $k_{st}/k_{nonenzymatic}$ (k_{st} is the single turnover rate constant)) and catalytic proficiencies (catalytic proficiency = $(k_{cat}/K_m)/k_W$ (k_w is the nonenzymatic bimolecular rate constant for *N*-glycoside hydrolysis)), with catalytic proficiency taking into account substrate binding, gave surprisingly similar values for modified and normal purines. This data suggests that enzyme efficiency is not a function of specific contacts the glycosylase makes with the base substrate, but perhaps a

consequence of the chemical instability of a particular substrate. AlkA's ability to excise normal purines from the DNA base stack (albeit at a much slower rate than damaged bases); is further highlighted by an increase in mutation frequency ascribed to an increase in AlkA expression (*23*). This excision is particularly efficient when the purine is mismatched. Mismatched base pairs may introduce disruptions to base stacking interactions and hydrogen bonding, encouraging base flipping. With regard to pyrimidine bases, AlkA seems to offer less catalytic assistance to these structures (*21*). The lack of any common structural features in the base region of AlkA's substrates not only highlight a non-base specific enzyme active site, but also give further support to the importance of interactions between the enzyme and the oxacarbenium ion to catalysis.

1.14 Transition State Theory and Kinetic Isotope Effects

Transition state theory holds that the transition state (TS) is the point of maximal energy along a reaction coordinate; accordingly, enzymes promote catalysis by binding to and lowering the energy of the TS. Enzymes bind the TS with greater affinity than either the reactants or products. Thus, in order to examine an enzyme's mechanism of catalysis, we must examine the TS. However, a TS only exists for a very short period of time, less than a single bond vibration (10^{-13}s). Herein lies the dilemma of how to study transition states that do not exist long enough to observe. Mathematically, there are 3 contributors to KIEs:

$$KIE = EXC \times MMI \times ZPE$$

The zero point energy (ZPE) is defined as the vibrational energy of an atom at 0 K. In a KIE, this value represents the contribution resulting from the difference in ZPE of isotopes at the initial state and at the TS. The ZPE comprises the largest contribution to a KIE. The excited state energy (EXC) represents the contribution from isotopic vibrational differences in excited molecules. The contribution from a change in mass and moments of inertia (MMI) results from an increase in mass and decrease in molecular motion, which stems from the presence of isotopically heavy atoms in KIE reactions (*48*).

Kinetic isotope effect (KIE) measurement is the only method that allows for direct transition state analysis, with accuracy in the best cases comparable to that of X-ray crystallography. A KIE is described as the ratio of rate constants, for reactions containing isotopically "light" and "heavy" substrates (KIE = $^{light}k/^{heavy}k$). KIEs are a vibrational phenomena that provide insight into changes in bonding an atom experiences as it proceeds from reactant to transition state. KIEs report on the vibrational environment of an atom as it proceeds from reactant to transition state. This vibrational environment includes bonding forces such as bond bends, stretches and torsions that affect the vibrational frequencies of a molecule. That is, KIEs are a vibrational phenomena that provide insight into changes in bonding an atom experiences as it proceeds from reactant to transition state. This vibrational information translates into the structural modifications between reactant and the transition state. KIE measurements use isotopically labeled substrates to measure changes in a given atom's vibrational environment. When an atom in the reactant molecule is replaced with its heavier isotope, the result is a change in the vibrational frequency at that site in the reactant; giving the heavy isotope a lower vibrational potential energy relative to the light isotope. At the

transition state, if the bonding environment of this position becomes more relaxed as a consequence of, e.g., sp^3 to sp^2 hybridization changes or bonds breaking, the potential energy differences between the light and heavy isotopes will be reduced in the TS relative to the reactant (Figure 1.10). If the vibrational environment of the atom becomes looser at the TS, the zero point energies will decrease for both isotopes, but it will decrease more for the light isotope. This makes its activation energy lower than the heavy isotope. Consequently, the light isotope reacts faster, conferring a normal KIE value (KIE >1) (Figure 1.10a). If the bonding environment of this atom becomes increasingly rigid at the transition state (a consequence of bond formation), the heavier isotope will react faster as a result of a lower activation energy barrier relative to the light isotope, giving an inverse KIE value (KIE<1) (Figure 1.10b).

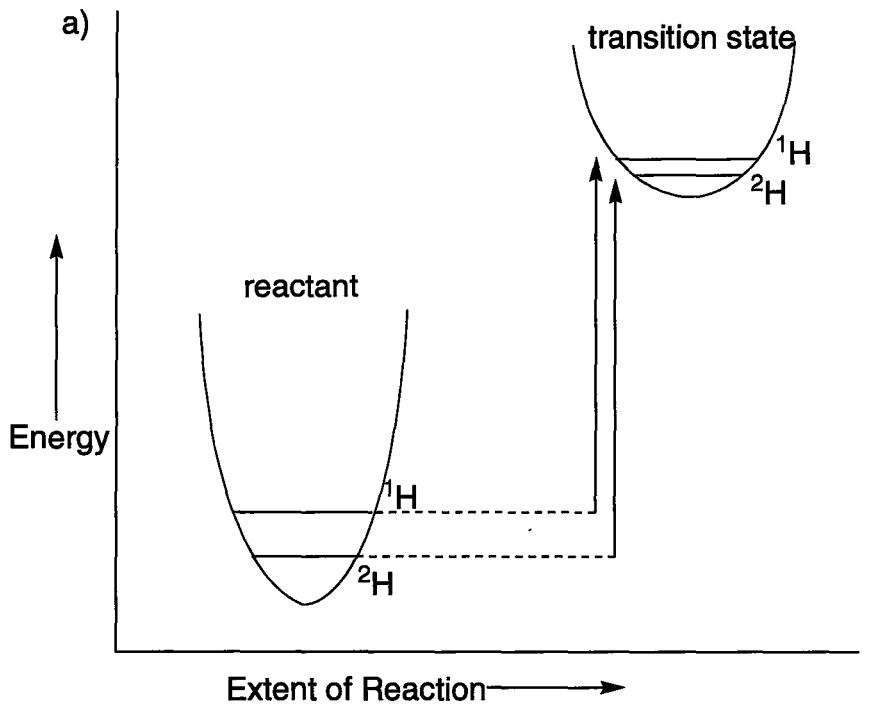

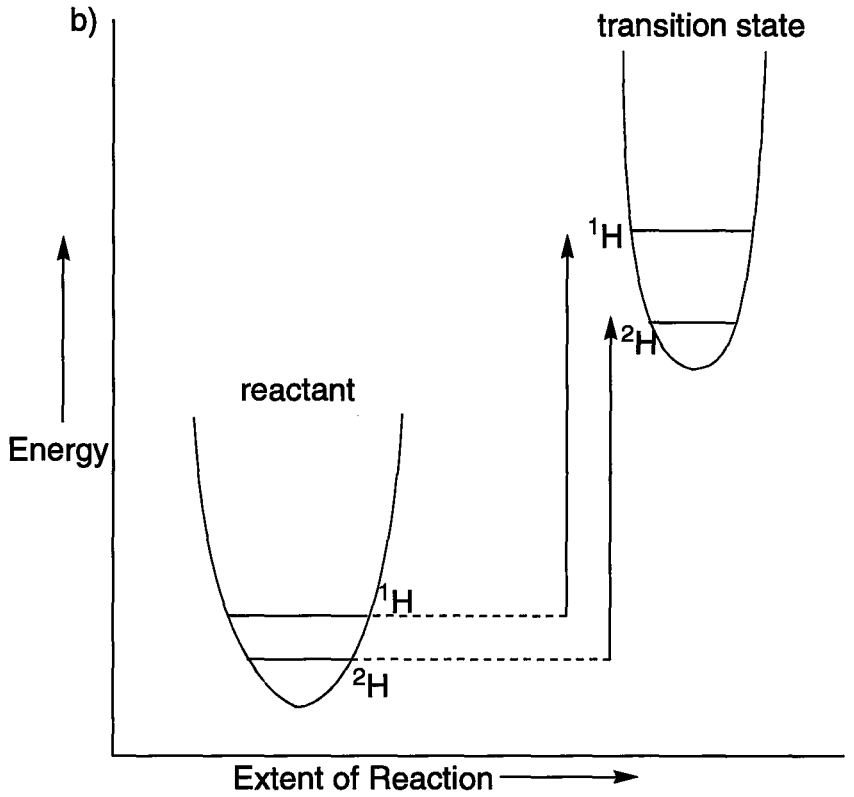

Figure 1.10. ZPE diagrams. The wells represent the vibrational energy for C-H stretching. (a) A normal isotope effect (b) An inverse isotope effect.

There are two types of KIEs. A primary KIE reflects the changes in the bonding environment of atoms directly involved in bond breaking and making. Conversely, secondary values describe the vibrational changes of atoms not directly involved in chemical steps.

KIE measurements allow for the distinction between a highly dissociative A_ND_N reaction pathway and stepwise D_N*A_N mechanism (*49*). This distinction arises from the contribution of the reaction co-ordinate motion to a KIE. The reaction co-ordinate

motion is a vibrational frequency that lacks a restoring force. That is, it represents motion along the reaction co-ordinate away from the TS; either forward to the products or back to the reactants. The contribution of the reaction co-ordinate motion gives the large primary KIE values typical of synchronous A_ND_N mechanisms. Moderate primary KIE values are suggestive of highly dissociative A_ND_N mechanisms, while smaller primary KIE values are indicative of (step-wise) $D_N{*}A_N$ reactions (Table 1.1).

Table 1.1. Primary KIE values for various mechanisms of N-glycoside hydrolysis (*22*).

Primary 1'-^{14}C KIE	**Reaction Mechanism**
≥ 1.13	Synchronous A_ND_N
1.025-1.06	Dissociative A_ND_N
1.01-1.02	$D_N{*}A_N$

KIEs can be measured using either competitive or noncompetitive methods (*50*). The noncompetitive method involves measuring of rate constants for reactions of light and heavy substrates independently, then taking the ratio of rate constants to give the KIE. The competitive method involves using a mixture of light and heavy substrates that compete as reactants. As the faster reacting isotopic substrate becomes enriched in the product, the isotope ratio will change. By comparing the isotope ratio of the residual substrate in reactions taken to 50% completion with the isotope ratio of unreacted substrates (or comparing the isotope ratio of the products in a 50% reaction to the isotope ratio of the products of a 100% reaction), the KIE at a given position can be determined. While the noncompetitive method allows for an extensive kinetic analysis of a given

reaction, the competitive method is preferable for TS studies, as isotope discrimination reports KIE values with a large degree of precision.

2.0 MATERIALS AND METHODS

2.1 Wild-type AlkA Purification

BL21* (DE3) cells (or JM101 cells) were transformed with pKEN2·alkA by electroporation. Cells were incubated for up to 2 h in SOC media at 37°C with shaking, then 100 to 200 μL aliquots were plated onto LB-agar plates containing 50 μg/mL ampicillin. The plates were incubated overnight at 37°C. Single colonies were selected from the plates and placed in 1 mL of sterile LB containing 50 μg/mL ampicillin. These 1 mL cultures were grown for 8 hours, and then used to inoculate 50 mL overnight cultures of sterile LB containing 50 μg/mL ampicillin. The 50 mL cultures were used to inoculate 1 L cultures containing 50 μg/mL ampicillin. The 1 L cultures were grown at 37°C until an OD_{600} of 0.6-0.8 was observed, and then IPTG was added to 0.1 mM final concentration to induce AlkA expression. The cultures were allowed to grow for an additional 4 h, at which point cells were harvested by centrifugation at 5000 × g for 20 min (at 4°C). Pellets were resuspended in lysis buffer A (50 mM Tris-Cl pH 8.6, 10 mM ethylenediaminetetraacetic acid (EDTA), 5% glycerol, 50 mM β-mercaptoethanol, 100 μM Benzamidine-HCl and 1 mg/mL phenylmethylsulphonyl fluoride (PMSF)). Prior to cell lysis, 1 mL of protease inhibitor cocktail (Sigma, 115K4098) was added to each resuspended pellet. Cells were lysed via French Press at 10 000 psi. Following cell lysis, an additional 2 mL of protease inhibitor cocktail was added to each cell lysate. Cell lysates were centrifuged at 30 000 × g for 30 min at 4°C. The supernatants were passed through a 0.45 μm filter, and an additional 1 mL of inhibitor cocktail was added to each clarified lysate. (The following chromatographic steps were carried out on an AKTA FPLC system with A_{280} detection at 4°C). Anionic

proteins and DNA were removed from AlkA by loading lysates onto a 75 mL DEAE column (equilibrated in lysis buffer A) and washed with 1-2 column volumes of lysis buffer A, to elute the protein. Collected fractions were analyzed via SDS-PAGE, following the method of Laemmli (*51*). Samples were mixed with 2× loading dye (63 mM Tris-HCl pH 6.8, 25% glycerol, 5% β-mercaptoethanol, 2% SDS, and 0.01% bromophenol blue) and heated at 95°C for 5 min. Samples were run on a 4% stacking gel and 15% resolving gel, with electrophoresis running buffer consisting of 25mM Tris, 192 mM glycine, and 0.1% SDS, using a Mini-Protean 3 electrophoresis cell (Bio-Rad Laboratories). Gels were subsequently stained with Coomassie blue stain (50%, MeOH, 40% water, 10% acetic acid, 0.05% Coomassie Brilliant Blue R250) for 25 – 30 min and de-stained in destaining solution (53% water, 40% methanol and 7% acetic acid overnight). Fractions containing AlkA were pooled and concentrated under N_2 (g) (at 4°C) using an Amicon ultrafiltration cell equipped with an YM10 regenerated cellulose membrane (molecular weight cutoff: 10 000, Amicon Bioseparations). Pooled fractions were applied to a SP-Sepharose column (equilibrated with lysis buffer A). The column was washed with at least 3 column volumes of lysis buffer A followed by 3 column volumes of 80 mM NaCl in lysis buffer A. A gradient of 80 mM to 350 mM NaCl in lysis buffer A over 5 column volumes was applied to the SP-Sepharose column. AlkA eluted between 163 mM and 222 mM NaCl. Fractions containing AlkA were verified with SDS-PAGE. AlkA containing fractions were concentrated under N_2 (g) and the concentrated sample was then applied to a heparin-Sepharose column equilibrated with 100 mM NaCl in lysis buffer A. A gradient of 100 mM to 700 mM NaCl (in lysis buffer A) over at least 9 column volumes was applied to the heparin-Sepharose column. AlkA

eluted under high salt conditions and fractions containing the protein were verified via SDS-PAGE.

2.2 AlkA_TEV_HIS and AlkA_HIS Purification

Plasmids (pET-24a_AlkA_TEV_HIS and pET24a_AlkA_HIS, Dr. O'Brien) containing the *alkA* gene with a C-terminal (cleavable or non-cleavable) histidine tag were transformed into BL21* (DE3) cells via electroporation. Transformations were incubated at 37°C for 1 h (in SOC media) and then (100 to 200 µL) were plated on LB agar plates containing 50µg/mL kanamycin. Plates were incubated at 37°C overnight. Single colonies were chosen to inoculate 1 mL of LB media containing 50µg/mL kanamycin. 1 mL cultures were grown for 8 h, at which time they were used to inoculate 50mL of LB medium containing 50µg/mL kanamycin. These 50 mL cultures were grown overnight at 37°C. The overnight cultures were used to inoculate 1 L cultures containing 50 µg/mL kanamycin, which were grown at 37°C to an OD_{600} of 0.4 to 0.6. Subsequent protein expression was induced by the addition of IPTG to 1 mM. Cultures were incubated for an additional 4 h upon induction and subsequently harvested via centrifugation at 5000 x g for 20 min at 4°C. Cell pellets were resuspended in lysis buffer B (50 mM Tris-Cl pH 7.5, 150 mM NaCl and 20mM imidazole). Prior to lysis, benzamidine and PMSF were added to the cell pellets to a final concentration of 1 mM. 50 – 100 U of DNase was also added to the cell pellets. Cell lysis was carried out via French Press at 10 000 psi. Cell debris was pelleted via centrifugation at 30 000 x g for 30 min at 4°C. The supernatant was then filtered using 0.45µm syringe filters. The clarified lysate was loaded onto a 1mL Ni-Sepahrose affinity column using a syringe pump (0.5 – 1 mL/min). The protein was eluted using a step-wise gradient on an AKTA

FPLC system with A_{280} detection. The column was first washed with lysis buffer B until the A_{280} returned to baseline. This wash removed any unbound protein from the column. Next, an 80 mM imidazole wash was applied to column until the A_{280} returned to baseline, in order to remove any protein non-specifically bound to the column. Finally, histidine tagged AlkA was eluted by applying lysis buffer C (50 mM Tris-Cl pH 7.5, 150 mM NaCl 500 mM imidazole) to the column until the A_{280} returned to baseline. Fractions containing AlkA were verified using SDS-PAGE (as previously described), and subsequently concentrated and exchanged (under N_2(g) as described above) into a storage buffer (20 mM NaHepes pH 7.5, 100 mM NaCl, 1 mM DTT, 0.2 mM EDTA). Samples of the protein fused to a cleavable His-tag were mixed with TEV protease (a gift from Dr. Junop) and 10X TEV reaction buffer at room temperature for 4 h, to cleave the histidine tag. The protein was exchanged into lysis buffer B and applied to a nickel-affinity column using a syringe pump, to remove the histidine-tagged TEV protease. AlkA eluted in the flow through and was subsequently exchanged (under N_2 (g)) into storage buffer for storage at -80°C. AlkA concentration was determined from the A_{280} measurements.

2.3 dITP Synthesis

dITP synthesis was performed following the one-pot enzymatic synthesis as described in the literature (*52, 53*), with some slight modifications.

2.3.1 ATP and dATP Synthesis

The analytical and preparative reverse phase chromatography described in the following section was performed on a Waters 600 liquid chromatography system, outfitted with a dual wavelength UV detector. Buffer solutions were filtered through

0.45 μm nylon membranes (Whatman) prior to use. The ^{14}C- and ^{3}H – labeled glucoses (American Radiolabeled Chemicals) used in the following synthesis were in 90% ethanol and lyophilized prior to use. The enzymes used in the following synthesis were purchased from Sigma, with the exception of phosphoribosyl pyrophosphate synthetase (PRPPase), adenine phosphoribosyltransferase (APRTase) and ribonucleoside triphosphate reductase (RTRase), which were previously purified from overexpressing *E. coli* strains as described by Joe McCann (*54*).

10 μCi of [6-^{14}C]glucose (in a final reaction volume of 182 μL) or 25 μCi of [2-^{3}H]glucose (in a final reaction volume of 22.5 μL) were added to a reaction mixture containing 50 mM glycylglycine, 50 mM potassium phosphate pH 7.8, 10 mM $MgCl_2$, 50 mM KCl, 5 mM DTT, 100 μM ATP, 3.2 mM adenine, 20 mM PEP and 5 mM NADP. To the reaction mixture 20 U/mL of myokinase, 7 U/mL of glucose-6-phosphate dehydrogenase, 1 U/mL of 6-phosphogluconic dehydrogenase, 5 U/mL of spinach phosphoriboisomerase, 25 U/mL of rabbit muscle pyruvate kinase, 1.5 U/mL of PRPPase and 0.6 U/mL of APRTase were added. Finally, the 2 U/mL of hexokinase was added to the mixture to initiate the reaction. ATP formation was monitored via HPLC. 20 μL aliquots were heated at 95°C for 5 min and centrifuged briefly to pool the liquid. The samples were diluted to 150 μL and injected onto an analytical C18 reverse – phase HPLC column (ID Supercosil LC-18-T column, 25 cm × 4.6 mm, 5μm particle). The reaction was monitored using dual wave absorbance at 260 and 280 nm, under isocratic conditions of 55% A (30% MeOH, 70% potassium phosphate pH 7.2, 4 mM tetrabutyl ammonium sulphate): 45% B (potassium phosphate pH 6.0, 4 mM tetrabutyl ammonium

sulphate) at 0.75 mL/min. The reaction was incubated at 37°C for 4 h, after which time HPLC analysis indicated that the formation of radiolabeled ATP had leveled off.

DTT and coenzyme B_{12} were added directly to the reaction to final concentration of 25 mM and 20 μM, respectively. The reaction was degassed under vacuum for 10 min and flushed with N_2. The degassing and flushing steps were repeated 3 times in the dark. RTRase was added to the reaction to a final concentration of 2.4 μg/μL. The reaction was degassed and incubated in the dark for 2 h at 37°C. The reaction was heated at 95°C for 5 min and centrifuged for 5 min at 15 000 x g to precipitate the denatured proteins. dATP was purified from the supernatant using C18 reverse phase HPLC (Waters column, 25 cm × 4.5 mm, 5μm particle). A gradient of 99% A and 1% MeOH to 84% A and 16% MeOH over 60 min (where A is 50 mM triethylammonium acetate pH 6.0) was used along with dual wave absorbance of 260 and 280 nm, and a flow rate of 1 mL/min.

2.3.2 dITP Synthesis

Purified dATP was dissolved in 10 mM sodium citrate pH 6.5, to a final concentration of 88.9 μM. AMP deaminase (Sigma) was added to a final concentration of 0.06 U/mL, and the reaction was incubated at 25°C for 1 h. The reaction was stopped by heating the solution at 95°C for 5 min and centrifuging for 10 min at 14 000 rpm. dITP was purified using C18 reverse phase HPLC (Waters column, 25 cm × 4.5 mm, 5μm particle). A gradient of 99% A and 1% B to 84% A and 16% B over 60 min (where A is 50 mM TEAA pH 6.0 and B is methanol) was used along with dual wave absorbance of 260 and 280 nm, and a flow rate of 1 mL/min.

2.4 5'- 33P labeling of DNA Stem-Loops

The forward labeling reaction contained 0.1 μM [γ - ^{33}P] ATP (Amersham), 1 μM DNA, 1 μM T4 kinase forward buffer (10X), and 1 μL of T4 kinase. The total reaction volume was 20 μL. The reaction was incubated for 0.5 h at 37°C. The reaction was subsequently placed on ice and stopped by the addition of 1 μL of 0.5 M EDTA (pH 8.0). The reaction was then diluted with 50 μL of 1X T4 kinase forward buffer. The reaction was extracted with an equivalent volume of chloroform. Labeled DNA was purified from unincorporated [γ-^{33}P] ATP by gel filtration, using Sephadex G-25 spin columns (GE Healthcare).

2.5 AlkA Activity Assay

The total enzyme concentration was 1 μM. The amount of ^{33}P 5'-labeled substrate used in each reaction was enough to generate 500 000 cpm, while unlabelled substrate was added to bring the total concentration of substrate to 1, 2 or 4 μM. The reaction mixture contained 50 mM KOAc (pH 6.0), 50 mM KCl, 10 mM $MgCl_2$, 1 mM DTT and 0.1 mg/mL BSA. Reactions were incubated at 37°C. At each time point, a 10 μL aliquot of the reaction mixture was added to 1 μL of 2 M KOH and heated at 95°C for 5 min. 10 μL of 2× loading dye was added to the sample. Substrates and products were resolved on an analytical (0.75 mm thickness) 20% denaturing polyacrylamide gel (as described for DNA concentration estimation). Gels were stored on a Molecular Dynamics phosphorimager (storage phosphor autoradiography) screen overnight. The phosphor imager screens were subsequently read using a Typhoon imaging system, and the resulting autoradiograms were analyzed using ImageQuant 5.1 software. Reactions

containing no AlkA were used to identify background phosphorescence, and reaction extent was corrected using this value. The extent of the reaction was determined using equation 2.1,

$$f(\text{rxn}) = \frac{P_{prod} - P_{prod,0}}{P_{total}} \qquad (2.1)$$

where P_{prod} is the phosphorescence observed in the product at a given time point, P_{total} is the phosphorescence observed in both the substrate and product at a given time point, and $P_{prod,0}$ is the phosphorescence observed in the product at $t = 0$.

2.6 Primer Purification

The C18 and G19 template and primer were chemically synthesized by Mobix and diluted to 1.2 – 1.4 mM. The strands were loaded onto 20% denaturing polyacrylamide gel and purified over 2 – 4 lanes, using a 1.5 mm thick gel. Samples were mixed with 2× urea loading dye (7M urea, 20% sucrose (w/v), 1% SDS (w/v), 0.5% bromophenol blue (w/v) and 0.5% xylene cyanol (w/v)). Gels were run using TBE (89 mM Tris-Cl, 89 mM boric acid and 2 mM EDTA) electrophoresis running buffer at 1000 V, until the xylene cyanol band was between 5 and 7 cm from the bottom of the gel. The bands were visualized using UV shadowing, cut from the gel and placed in a sterile 50 mL Falcon tube. The bands were crushed by vortexing and using a sterile pipette tip. 10 mL of TE (10 mM Tris-Cl pH 8, 1 mM EDTA pH 8) buffer was added to the tube for every 2.5 g of gel pieces. The suspension was vortexed for 2 min and frozen at -80 °C. The suspension was rapidly thawed at 90°C and mixed overnight at 37 °C. The gel suspension was filtered through 0.45 μm syringe filters (Pall). Sodium acetate (pH 5.1)

was added to the solution to a final concentration of 0.3 M. 2.5 – 3× volume equivalents of 100% cold ethanol were added to the mixture, which was subsequently placed at -80°C for 1 h to precipitate the DNA. The precipitate was pelleted by centrifugation at 25 000 × g for 20 min at 4°C. The supernatant was decanted and the pellet was lyophilized to dryness. The resulting pellet was re-suspended in water and desalted using Sephadex G-25 spin columns. DNA concentration was determined from the A_{260} measurements and by running analytical 20% denaturing polyacrylamide gels (0.75 mm thickness). Gels were prepared and run as described above, except gels were run at 1000 V until the bromophenol blue band had migrated approximately two-thirds of the way down the gel. Gels were stained using ethidium bromide stain (0.5 μg/mL) for 20 – 25 min and visualized using a UV light box. Fluorescence intensities of sample bands were compared to fluorescence intensities of standard bands containing a known quantity of the primer or template DNA. DNA purity was also assessed using these preparative gels.

2.7 ATI26 Synthesis

In a 1000 μL reaction volume, 30 μM G19 primer, 30 μM C18 template, 30 μM [5'-^{14}C]dITP, and 25 U/μl of MMLV reverse transcriptase (Invitrogen) were mixed in a reaction buffer containing 50 mM Tris-HCl pH 8.3, 75 mM KCl, and 3 mM $MgCl_2$. The reaction was incubated for 4 h at 37°C, then 250 μM of unlabelled dITP, 250 μM dTTP, and 250 μM dCTP were added, and the reaction was incubated at 37°C for an additional 3 h. The reaction mixture was lyophilized to a volume of approximately 200 μL and 3X the volume of cold 100% EtOH was added, to precipitate the DNA. The mixture was allowed to stand at -20°C overnight. The mixture was then centrifuged at 20 000 x g for

20 min to pellet the DNA. The supernatant was decanted and the pellet was lyophilized to dryness. The pellet was re-dissolved in 100 μL of ddH_20, desalted, and the DNA was then purified over 10 lanes on 20% denaturing polyacrylamide gel. The DNA was visualized using UV shadowing and the bands were cut from the gel. The bands were placed in a sterile 15 mL Falcon tube and crushed using a sterile pipette tip. For every 300 mg of gel, 1.2 mL of TE buffer was added to the Falcon tube. The mixture was vortexed for 2 min, and frozen at -80°C. The mixture was then thawed rapidly at 90°C and mixed overnight at 37°C with shaking. The gel suspension was loaded into empty spin columns and spun for 10 min at 14 000 rpm in a microcentrifuge (twice). The flow through was pooled and lyophilized to approximately 200 μL. Sodium acetate (pH 5.1) was added to the sample to a final concentration of 0.3 M. Glycogen (20-50 μg) was added to the mixture, followed by 1 mL of 100% cold ethanol. The solution was allowed to stand at -20°C to precipitate the DNA. The mixture was subsequently spun at 20 000 × g for 20 min to pellet the DNA. The supernatant was removed and the pellet was lyophilized to dryness. The pellet was dissolved in 150 μL of ddH_20 and desalted on a Sephadex G-25 spin column. The DNA concentration was determined from the A_{260} values.

2.8 [1'-3H] KIE Measurement

2.7×10^5 cpm of [1'-^{3}H]ATI26 and 2.2×10^5cpm of [5'-^{14}C]ATI26 were mixed with 50 mM KOAc, 50 mM KCl, 10 mM MgCl2, 1 mM DTT, and 0.1 mg/mL BSA. The final reaction volume was 4 mL. The reaction was split into 1/3 (0% reaction) and 2/3 (50% or partial reaction). 2 μM AlkA and hAPE1 (to a final concentration of 0.3 U/μL) were added to the partial reaction only. The reactions were incubated at 37°C for 6.5-7 h.

Subsequently, 0.2 M KOH and 30 mM ETDA were added to both reactions. The reactions were heated at 95°C for 10 min. The 0% and partial reactions were purified using anion exchange chromatography (on a Waters 600 HPLC system equipped with a MonoQ 5/5) in 3 equal injections and 6 equal injections, respectively. During each injection the β-elimination product and residual substrate were collected directly into pre-weighed scintillation vials. To each vial, 250 µL of 1 M potassium phosphate pH 6.0 was added and the liquid weight of the vial was divided into two equal halves. Neutralized elution buffer was added to each vial until all liquid weights were balanced. 20 mL of scintillation fluid (Liquiscint, National Diagnostics) was added to each sample vial and all samples were counted using dual channel analysis on a Beckman LS 6500 liquid scintillation counter. A blank sample (used to determine background counts) was prepared by injecting 2 µM of unlabelled ATI26 onto the MonoQ 5/5 column. The peak was collected and treated as described above. Channels (or energy windows) were selected on the scintillation counter such that all ^{3}H counts occurred in Window_1, while only ^{14}C counts occurred in Window_2. A ^{14}C standard was used to find the proportion of ^{14}C counts occurring in Window_1. Prior to counting, 0.5 µL of [2'-^{14}C]glucose was added to one of the vials, to serve as a ^{14}C standard. ^{3}H and ^{14}C counts were determined for each sample using equations 2.2 and 2.3, following background correction.

$$^{3}H \text{ counts} = \text{Window\_1} - \left[\text{Window\_2} \times \left(\frac{\text{Window\_1}}{\text{Window\_2}} \right)^{^{14}C \text{ standard}} \right] \qquad (2.2)$$

$$^{14}C\ counts = Window\_2 + \left[Window\_2 \times \left(\frac{Window\_1}{Window\_2} \right)^{^{14}C\ standard} \right] \qquad (2.3)$$

The KIE was calculated using equation 2.4,

$$KIE = \frac{\ln\left[\frac{(1 - f)(1 + 1 / R_o)}{(1 + 1 / R_i)}\right]}{\ln\left[\frac{(1 - f)(1 + R_o)}{(1 + R_i)}\right]} \qquad (2.4)$$

where R_0 represents the ratio of cpm in the light substrate (in this case the ^{14}C cpm) divided by the cpm in the heavy substrate (in this case the ^{3}H cpm) from the purified 0% reaction and R_i represents the ratio of cpm in the light substrate divided by the cpm in the heavy substrate from the purified partial reaction. The value *f* represents the extent of the reaction, as determined from comparing the cpm from the product peak with the cpm from the residual substrate peak, for all 6 purifications of the partial reaction. Equation 3 also corrects for the fact that the residual substrate is depleted in the faster reacting isotopologue.

3.0 RESULTS

3.1 Determining a Substrate

In previous studies of AlkA activity, double stranded DNA substrates were used (*21*). However, for TS analysis using KIE measurements a double stranded substrate is not viable because incomplete annealing results in substrates that can only react to approximately 90% completion. Instead a stem-loop substrate is preferred as reactions with this type of DNA substrate can proceed □ 99% completion.

Enzyme activity was measured against 7 stem-loop substrates, containing adenine mismatches with adenine, guanine and cytosine; or hypoxanthine mismatches with adenine, guanine, cytosine and thymine. These stem-loop substrates consisted of an 11 base pair stem containing a centrally located mismatch, and with three thymine bases comprising the loop. In addition, enzyme activity was assayed against two stem-loops containing hypoxanthine in the loop of the DNA substrate. In substrate **1j** (Figure 3.1), the central thymine in the loop was replaced with hypoxanthine. In substrate **1k** (Figure 3.1), the 3 thymine residues of the loop are replaced with the sequence GIGA. As well, excision was assayed against stem-loop substrates containing an adenine or hypoxanthine bulge. These substrates consisted of a 3 thymine residue loop and an 11-base pair stem region containing a centrally located unpaired adenine or hypoxanthine base.

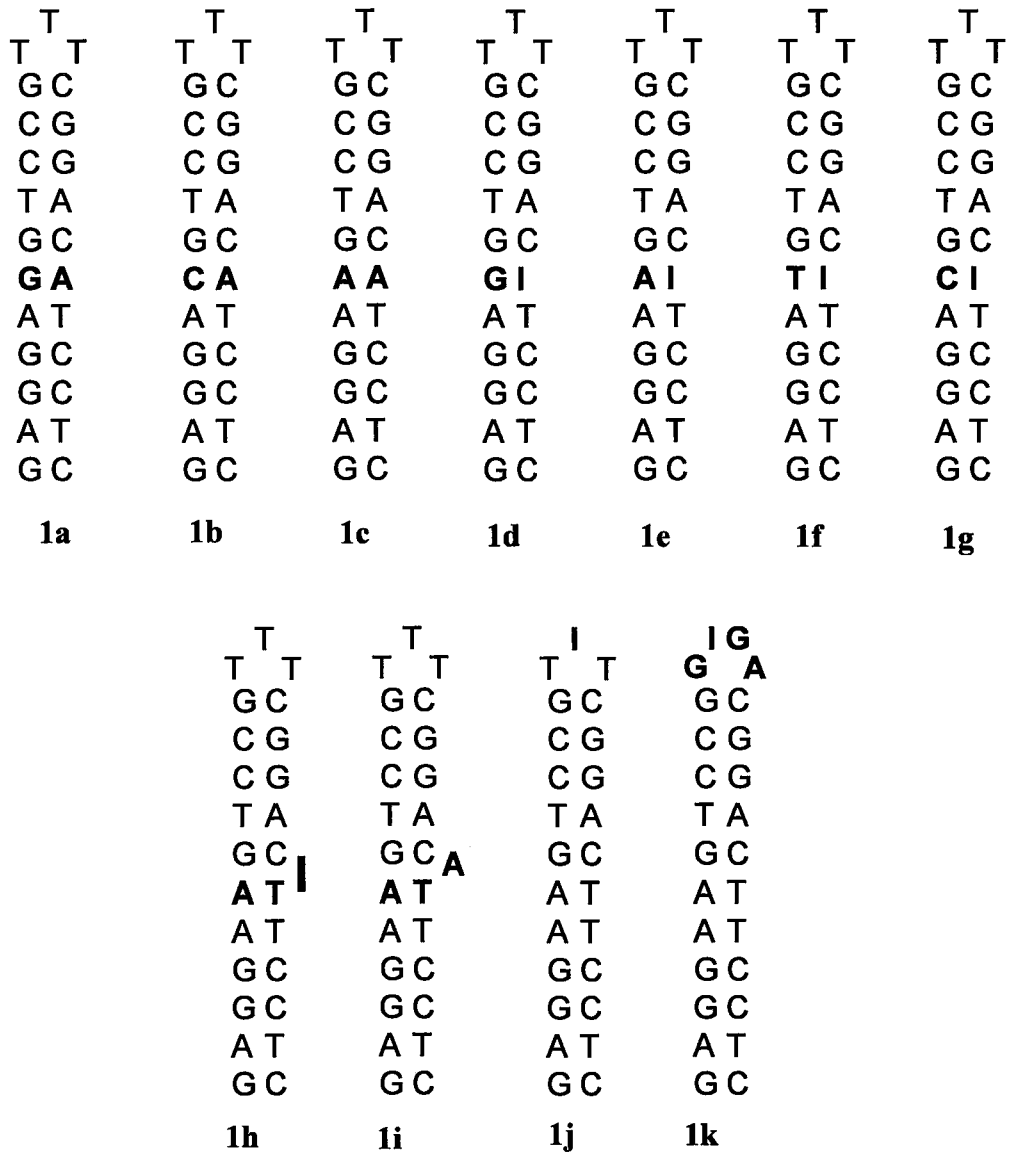

Figure 3.1. AlkA Stem-loop Substrates. AlkA activity was assayed against 11 stem-loop DNA structures, containing adenine and hypoxanthine mismatches, adenine and hypoxanthine bulge structures, and two substrates with hypoxanthine in the loop region.

All DNA stem-loop substrates were analyzed using Netprimer (Premier Biosoft) to ensure that any additional secondary structure formation (besides the desired hairpin) was minimal. The adenine mismatch substrates (**1a-1c**) and hypoxanthine loop

substrates (**1j** and **1k**) displayed no observable cleavage of the N-glycosidic bond, after seven days. However, base excision was observed with the inosine mismatch substrates (**1d-1f**). The T:I, A:I and G:I mismatched substrates were cleaved by wild type AlkA with similar rates of excision. Interestingly, the enzyme demonstrated no activity towards the C:I mismatch substrate, while a 25 base-pair double stranded substrate containing a centrally located C:I mismatch was shown to be cleaved by the enzyme.

The hypoxanthine bulge substrate was the only bulge substrate shown to be cleaved by the enzyme. Variations of this substrate, containing a longer stem region (15, 21, and 26 base pairs) were also assayed for N-glycoside hydrolysis by AlkA. No significant increase in base excision was observed with a longer stem region.

Table 3.1. Observed rates of excision for various substrates with wild-type, His-tagged and (cleaved His tag) AlkA.

Substrate/Enzyme	**Length of Stem**	**Observed Rate (min^{-1})**
ATI26 with WT AlkA	11	$2.6 \times 10^{-3} \pm 1.0 \times 10^{-3}$
ATI34 with WT AlkA	15	$4.2 \times 10^{-3} \pm 2.0 \times 10^{-3}$
ATI46 with WT AlkA	21	$2.5 \times 10^{-3} \pm 6.4 \times 10^{-4}$
ATI56 with WT AlkA	26	$4.2 \times 10^{-3} \pm 1.6 \times 10^{-3}$
ATI56 with Histidine tagged AlkA	26	$5.2 \times 10^{-3} \pm 1.3 \times 10^{-3}$
ATI56 with AlkA (His tag removed by TEV protease)	26	$3.3 \times 10^{-3} \pm 4.0 \times 10^{-4}$
TI25 mismatch with AlkA	11	$1.4 \times 10^{-4} \pm 1.3 \times 10^{-5}$
AI25 mismatch with AlkA	11	$1.3 \times 10^{-4} \pm 1.5 \times 10^{-5}$
GI25 mismatch with AlkA	11	$1.2 \times 10^{-4} \pm 1.5 \times 10^{-5}$
CI (25bp) ds with AlkA	N/A	6.0×10^{-3}

The hypoxanthine bulge was excised by AlkA 18- to 37-fold more efficiently than the hypoxanthine mismatched substrates. This excision efficiency is similar to that observed for double stranded substrates.

Excision efficiency of ATI26 was examined in the presence of human **ap**urinic/apyrimidinic **e**ndonuclease 1 (hAPE1) (Table 3.2). This endonuclease has been shown to enhance base excision of some DNA glycosylases, such as hOGG1. Enzyme activity monitored over 3 h demonstrated no increase in excision, in the presence of hAPE1. No increase in base excision was observed when the amount of hAPE1 was increased 3-fold (data not shown).

Table 3.2. The effect of hAPE1 on AlkA catalyzed N-glycoside hydrolysis.

+/- hAPE1	**Observed Rate (min^{-1})**
+ 0.3U/μL hAPE1	$5.4 \times 10^{-3} \pm 4.0 \times 10^{-4}$
- 0.3U/μL hAPE1	$5.6 \times 10^{-3} \pm 4.0 \times 10^{-4}$
+ 0.3U/μL hAPE1 no AlkA	No observed excision

3.2 [5'14C]- and [1'3H]dITP Synthesis

dITP synthesis involved the deamination of dATP generated using an enzymatic synthesis, as outlined in the following scheme (Scheme 3.1) (*52, 53*). The first part of this synthesis involves the generation of [5'-^{14}C]- and [1'-^{3}H]ATP from [6'-^{14}C]- and [2'-^{3}H]glucose. Control reactions demonstrated that the formation of ATP leveled off after 4 h of incubation, as previously reported [3]. The second part of this one – pot enzymatic synthesis involved the conversion of ATP to dATP. Typically conversion of ATP to dATP gave 60 and 70% yields (based on peak areas for ATP and dATP) upon

incubation with RTRase and coenzyme B_{12} for 2 - 3 h. A representative chromatogram of the [1'-^{3}H]dADP purification is shown in Figure 3.3. [1'-^{3}H]dADP eluted at 23.7 min, compared with 23.4 min for a dATP standard

Scheme 3.1

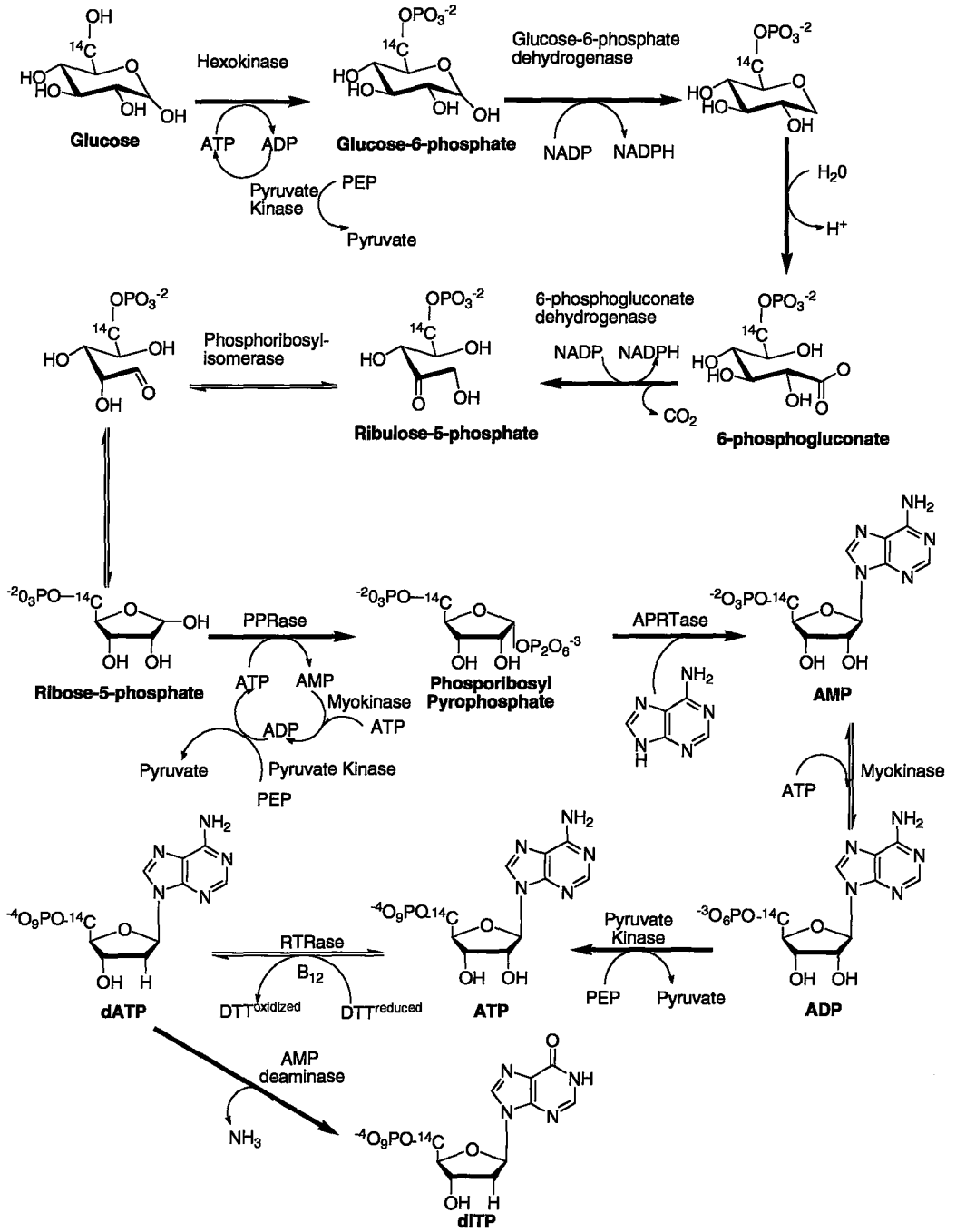

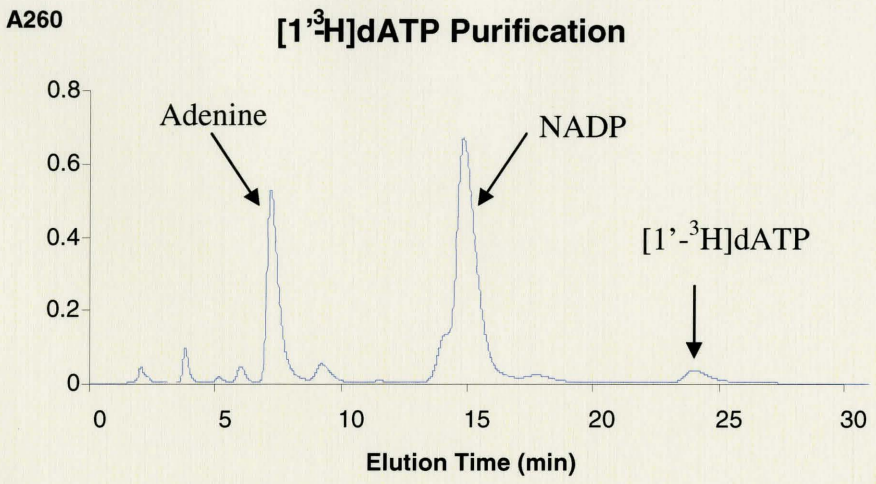

Figure 3.2. A representative chromatogram of the purification of [1'-^{3}H]dATP. [1'-^{3}H]dATP eluted at 23.7 min.

The purified [5'-^{14}C]- or [1'-^{3}H]dATP was subsequently incubated with AMP deaminase. Initially, the synthesis of dITP involved the conversion of dATP to dAMP using myokinase and glucose, followed by the deamination of dAMP (which was shown to also be a substrate for AMP deaminase) to dIMP, and finally the synthesis of dIMP to dITP using myokinase and pyruvate kinase. However, dATP was also shown to be a substrate for AMP deaminase, and we were subsequently able to synthesize dITP directly from the dATP generated using the one-pot enzymatic synthesis. The resulting [5'-^{14}C]- and [1'-^{3}H]dITP was purified using reverse phase chromatography with an average yield of 70-80%. A representative chromatogram is shown in Figure 3.4, outlining the purification of [5'-^{14}C]dITP reaction. [5'-^{14}C]dITP eluted at 14.8 min, corresponding to the elution of a dITP standard at 14.9 min.

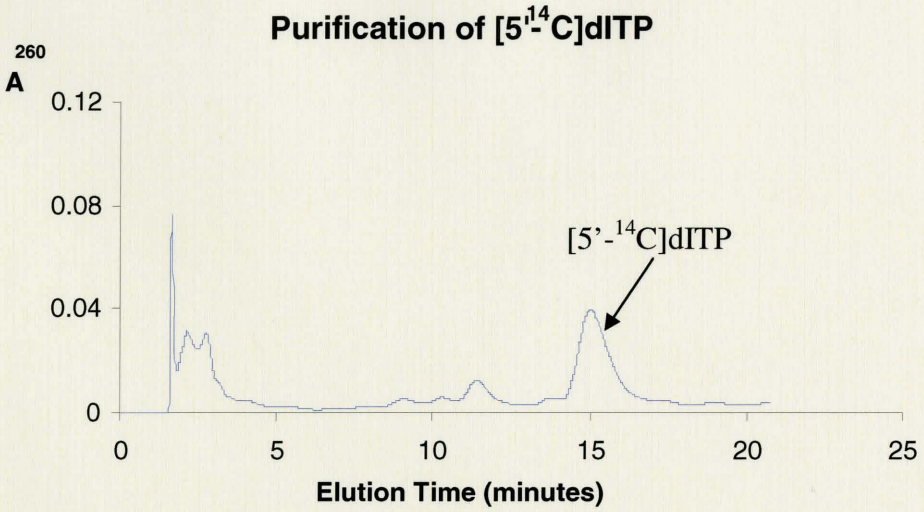

Figure 3.3. A representative chromatogram of the purification of [5'^{14}C]dITP. [5'^{14}C]dITP eluted at 14.8 min.

3.3 ATI26 Stem-loop Synthesis

3.3.1 Template and Primer Design

The G19 primer was designed to comprise the first 19 nucleotides of the stem-loop substrate from the 5' terminus (Figure 3.5). The first 11 bases comprise one half of the complementary stem. This is followed by the three thymine nucleotides, making up the loop. The remaining 5 nucleotides of the G19 primer make up part of the second half of the complementary stem. The incorporation of the radiolabeled dITP and the remaining 6 nucleotides necessary for a complementary stem region was directed by the C18 template oligonucleotide. The seventh base from the 5' terminus of the C18 template is cytosine which directs the incorporation of dITP.

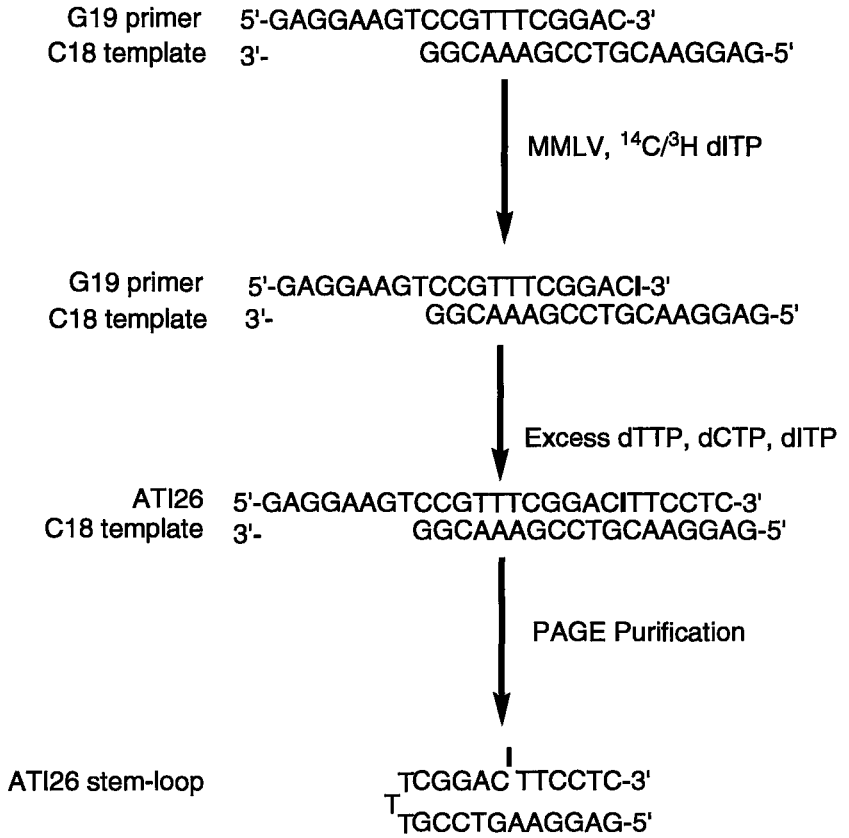

Figure 3.4. Synthesis of the ATI26 stem-loop. Labeled dITP is bolded in the stem-loop.

3.3.2 Incorporation of dITP

Control reactions for ATI26 synthesis demonstrated that dITP is incorporated exclusively opposite the cytosine residue, as indicated in Figure 3.6. The control reactions used an excess of unlabelled dITP during the first incubation (in comparison to the stoichiometric amounts used for labelled dITP incorporation). After a 2 h incubation period, the formation of a new band was observed using PAGE (Figure 3.6, lane 4). This band corresponded to a 20 base oligonucleotide, implying exclusive incorporation of dITP at one site in the stem-loop substrate.

1 2 3 4 5

Figure 3.5. Denaturing 20% PAGE analysis of the ATI26 synthesis showing: lane 1 - C18 standard, lane 2 - G19 standard, lane 3 - ATI26 standard, lane 4 - ATI26 synthesis after 2 h, showing the exclusive formation of a 20 base oligonucleotide, lane 5 – ATI26 synthesis after 4 h showing formation of a 26 base oligonucleotide.

The overall incorporation rate of dITP opposite cytosine was low relative to dGTP (Figure 3.7). In control reactions, MMLV activity was assayed using stoichiometric amounts of dGTP and dITP during the first 2 h incubation. dGTP was incorporated much more efficiently by MMLV after 2 h, as demonstrated by the strong band representing a 20 base oligonucleotide in lane 3. dITP incorporation and subsequent 20 – mer formation occurs much more slowly than dGTP incorporation as demonstrated by the faint band representing a 20 base oligonucleotide in lane 4. Lanes 5 and 6 indicate that the formation of a 26 base oligonucleotide does not differ significantly between the two reactions, suggesting that the formation of 20 base oligo (and subsequently a 26 base fragment) is facilitated via the addition of excess dITP during the latter 2 h incubation of the ATI26 stem – loop synthesis. Lanes 7 and 8 suggest that prolonged incubation does not encourage the formation of additional 26 – mer, though some G19 and G20 oligos still remain.

1 2 3 4 5 6 7 8 9

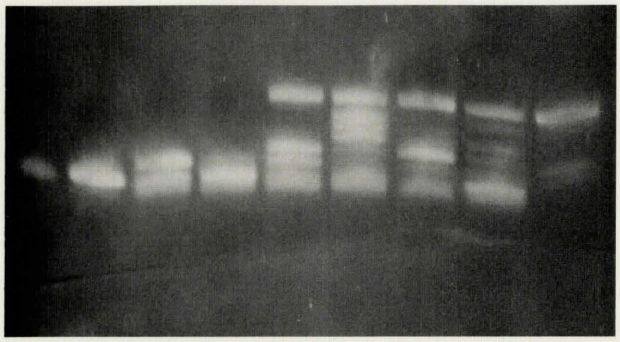

Figure 3.6. Denaturing 20% PAGE analysis of the ATI26 synthesis showing: lane 1 – C18 standard, lane 2 – G19 standard, lane 3 – ATI26 synthesis using dGTP after 2 h, lane 4 –ATI26 synthesis using dITP after 4 h, lane 5 - ATI26 synthesis using dGTP after 4 hr, lane 6 - ATI26 synthesis using dITP after 4 h, lane 7 - ATI26 synthesis using dITP after overnight incubation, lane 8 - ATI26 synthesis using dITP after overnight incubation, lane 9 - ATI26 standard.

In an attempt to enhance dITP incorporation, control reactions were carried out with increasing amounts of MMLV. 10 U/μL, 25 U/μL and 50 U/μL of MMLV reverse transcriptase were used to synthesize G20 (and subsequently ATI26) (Figure 3.8). The 20 - mer bands observed in lanes 4 and 5 showed a fluorescent intensity greater than that of the 20 – mer band observed in lane 3, indicating that increasing amounts of MMLV encourage G20 formation. Interestingly, there was not a significant difference in the fluorescent intensities of the 20- mer bands in lanes 4 and 5, though 50 U/μL seemed to encourage the formation of the 26 base stem-loop, as shown by the strong (topmost) band in lane 8.

1 2 3 4 5 6 7 8

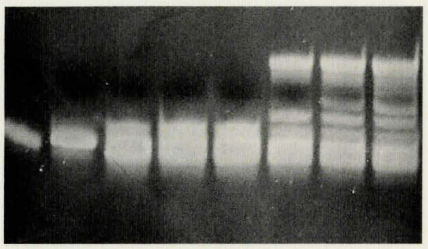

Figure 3.7. Denaturing 20% PAGE analysis of the ATI26 synthesis showing: lane 1 – C18 standard, lane 2 – G19 standard, lane 3 – ATI26 synthesis after 2 h with 10 U/μL, lane 4 - ATI26 synthesis after 2 h with 50 U/μL, lane 5 - ATI26 synthesis after 2 h with 25 U/μL, lane 6 - ATI26 synthesis after 4 h with 10 U/μL, lane 7 - ATI26 synthesis after 4 h with 25 U/μL, lane 8 - ATI26 synthesis after 4 h with 50 U/μL.

Overall radioactive yields using 25 U/μL ranged between 12 – 17% recovery. While still relatively low, this yield was better than that observed for reactions using 5 U/μL MMLV (1.3% radioactivity recovered). Previously reported yields for labeled GA25 synthesis using MMLV ranged from 20 to 60% recovery of radioactivity (*54*).

3.4 AlkA Purification

Initial attempts at purification of wildtype AlkA proved unsuccessful. While the protein was overexpressed in E.coli and migrated on SDS PAGE with a R_f value consistent with AlkA, subsequent purification of the protein from contaminants was limited as a result of inefficient separation of the protein on a cation exchange chromatography resin. The protein was observed to elute in the wash buffer along with contaminants. Various attempts to improve binding of the target protein proved unsuccessful and a sample of this protein demonstrated no activity when incubated with ATI26 and ATI56. It was hypothesized that this lack of activity was the result of a structural perturbation. Subsequent mass spectrometry (MS) analysis of the sample

revealed a major peak at 28466 Da, compared with the expected molecular weight of 31393 Da.

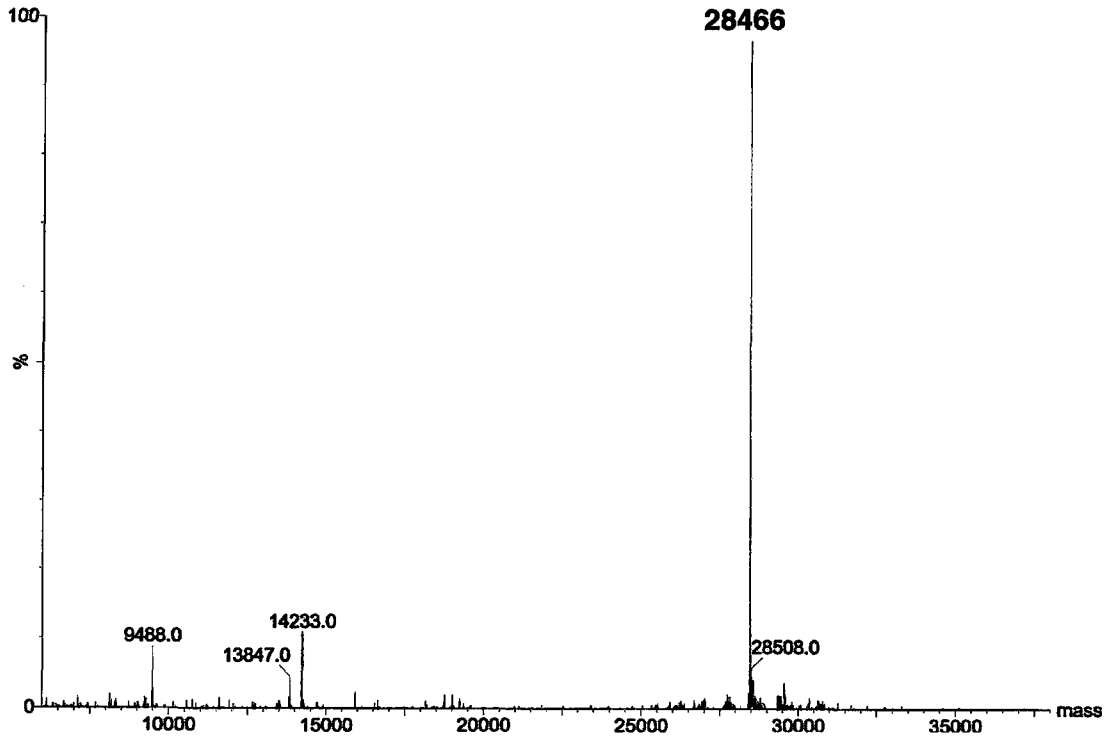

Figure 3.8. MS analysis of an AlkA sample purified on a DEAE cellulose anion exchange resin. The sample consists primarily of a sample with a molecular weight of 28466 Da.

The observed molecular weight was consistent with the removal of 24 amino acids from the C-terminus. This corresponds to cleavage C-terminal to an arginine residue, suggestive of trypsin-like protease activity. To minimize protein cleavage, protease inhibitor cocktail was added to the cell pellet prior to lysis, and to the cell lysate following lysis. The cocktail contained 4-(2-aminoethyl) benzenesulphonyl fluoride hydrochloride (ABESF), an irreversible serine protease inhibitor with a specificity similar to that of PMSF; though it is significantly more stable in aqueous solutions. The inhibitor cocktail also contained E-64 (an irreversible cysteine protease inhibitor), Bestatin (an

aminopeptidase inhibitor), Pepstatin A (an inhibitor of acid proteases) and EDTA (for inhibition of metalloproteases). In addition, PMSF concentration of the lysis buffer was increased 10-fold. As well, another trypsin inhibitor benzamidine-HCl was added to all buffers and the EDTA concentration of all buffers was increased 10-fold. While addition of the inhibitor cocktail improved binding of the AlkA protein to the cation exchange resin, activity assays with this sample of protein demonstrated cleavage of not only the inosine bugle, but of other sites on the stem-loop substrate. This additional cleavage was not observed with previously purified WT AlkA and subsequent mass spectrometry analysis revealed a predominant peak of 31584 Da, with smaller peaks observed at 31608 Da and 31757 Da (Figure 3.10).

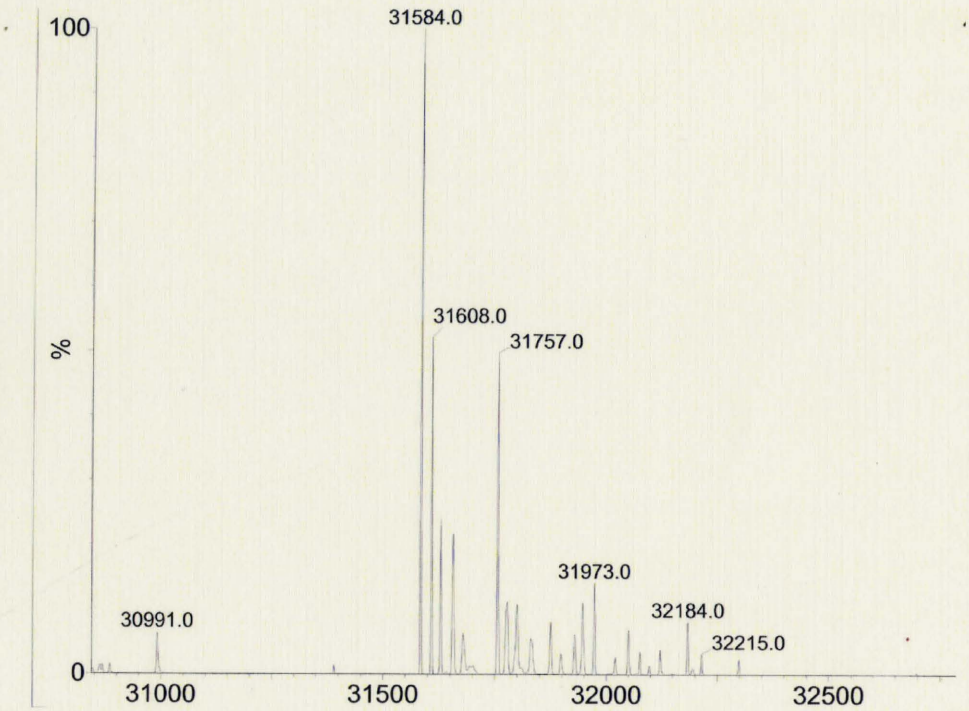

Figure 3.9. MS analysis of AlkA sample purified using protease inhibitor cocktail.

This was at least 191 Da higher than the expected molecular weight of 31393 Da. The average molecular weight of an ABESF adduct is 183 Da. The average molecular weight

difference between significant peaks was 179 Da. Thus it appears that AlkA was covalently modified by multiple ABESF adducts.

Efforts were made to purify modified AlkA proteins; one containing a hexa-histidine tag at the C-terminal, and another containing a hexa-histidine tag preceded by TEV protease recognition sequence (at the C-terminal). This latter modification allows for the cleavage of the histidine tag via TEV protease. Purification of these modified AlkA proteins was carried using Ni affinity chromatography and the histidine tag was cleaved via incubation with TEV protease. SDS-PAGE analysis confirms the cleavage of this TEV sequence, and activity assays with ATI56 demonstrate specific cleavage of the inosine bulge with rates of excision comparable to that of WT AlkA (see Table 1). Final protein yields were calculated from absorbance readings at 280 nm using the average of the calculated molar extinction coefficients generated by ProtParam Expasy software. The average protein yield was 116 μg of AlkA per litre of cell culture.

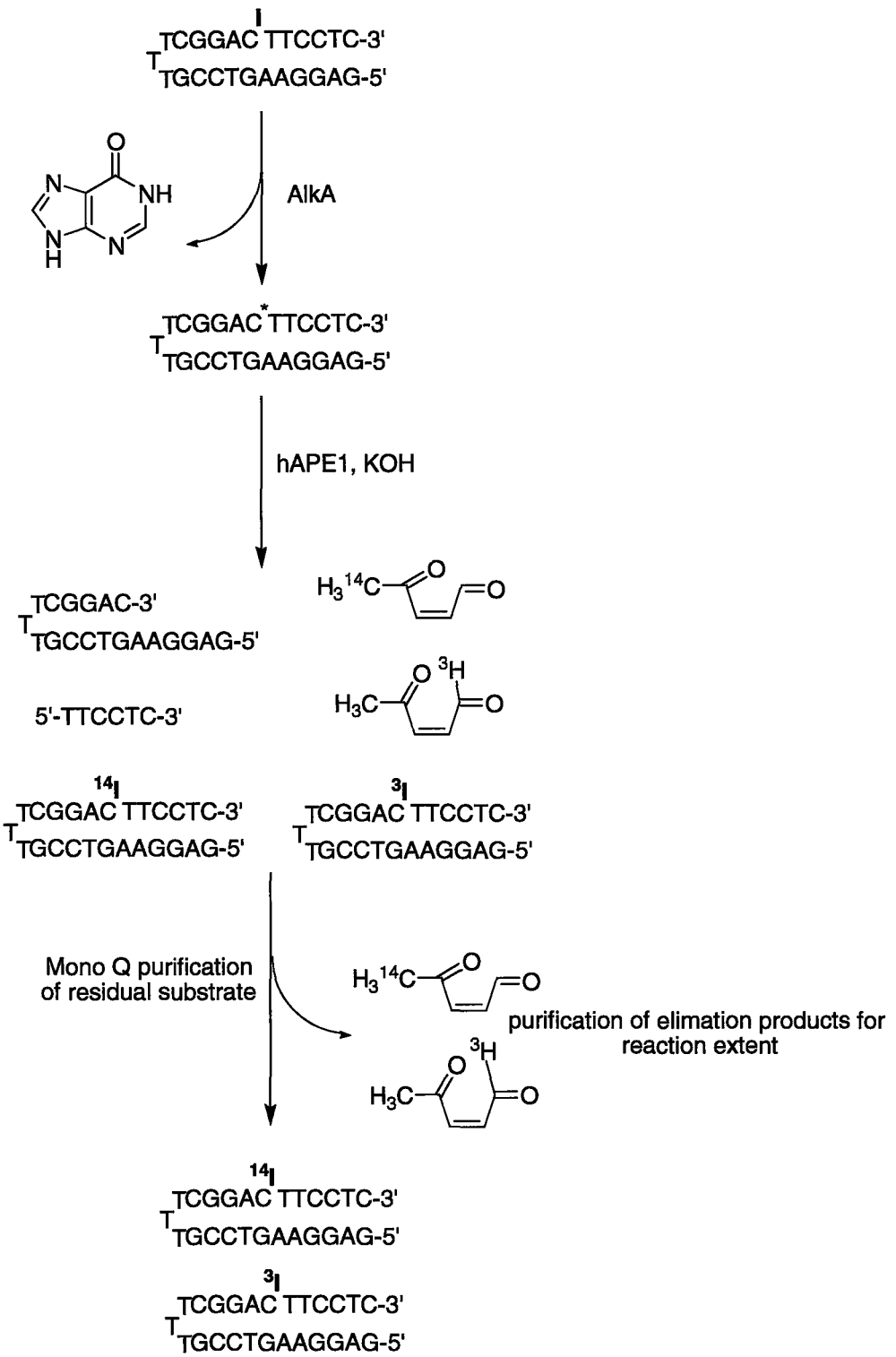

Figure 3.10. A schematic representation of the KIE reaction and purification of residual substrate from the partial reaction. The * represents an abasic site in the DNA substrate.

3.5 [1'- 3H] KIE Measurement

The [1'- ^{3}H] KIE was measured using the competitive method. The isotope ratio of the substrates in the 0% reaction was compared with the isotope ratio of the substrates in the 50% reaction. After AlkA cleaved the N-glycosidic bond, hAPE1 hydrolyzed the phosphodiester bond 5' to the abasic (AP) site. Control reactions with hAPE1 only demonstrated no cleavage of the ATI26 stem-loop substrate. The δ- and β-elimination reaction was then promoted by treating the reaction with base, and the residual substrate was purified on the HPLC using anion exchange chromatography (Figure 3.11). The products of the δ- and β-elimination reaction were collected within the first 5 minutes of the gradient to determine the extent of the reaction, while residual substrate eluted between 11 - 12 min.

The 1'^{3}H KIE was successfully measured once. The observed experimental value was 1.046 ± 0.009 after 12 cycles of counting (Scheme 3.2)

Scheme 3.2

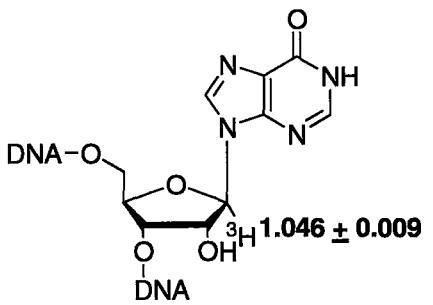

4.0 DISCUSSION

4.1 Substrate Design and ATI26 Synthesis

The stem-loop structure consists of an 11 base pair stem, containing a mismatch or bulge, connected by a triple thymine loop. This triple thymine loop has been shown previously to confer significant flexibility to the strand, enabling stem-loop formation (*55*). Initially each of the substrates shown in Figure 1 was analyzed using NetPrimer Software to examine the extent of additional secondary structure and dimer formation. The stem loop structures were designed so that the only secondary structure formed should be the stem-loop with the mismatch. There were no other significant predicted secondary structures. In principle, each oligonucleotide could form a double stranded dimer with itself; however given the short complementary sequences, the breaks in complementarity at the mismatch site and the TTT loop, plus the intrinsic entropic disadvantage to forming a double-stranded DNA, the stem-loop structure would be expected to be the dominant form. If double-stranded DNA were formed, the structure of the mismatch or bulge should be the same as the stem-loop, and the transition state, if it were cleaved, would also be expected to be the same. Analysis of substrates containing hypoxanthine was less reliable as the program does not recognize this base. Guanine was substituted in place of hypoxanthine for these structures, based on similar hydrogen bonding properties. The stem-loop type substrate is more favourable than a double stranded substrate for KIE measurements as it ensures that essentially all of the radiolabel is available for cleavage. Double stranded substrates demonstrate incomplete annealing, resulting in substrates that do not proceed past 90% reaction completion (*55*), thus

limiting the accuracy of KIE measurements that require the extent of reaction be able to proceed to > 99% completion. Control substrate synthesis reactions suggest that ATI26 synthesis was limited by the inefficient incorporation of dITP opposite cytosine by MMLV RT. Presently, enough radioactivity is recovered from each synthesis to successfully carry out a single KIE measurement. However, further optimization of the ATI26 synthesis is necessary to increase radioactivity recovery beyond 17%. Initial recovery following the precipitation of DNA from the synthesis reaction is approximately 75-85%. Subsequent to PAGE purification, final yields are 12 to 17% recovery. It is expected that losses in radioactivity are incurred as a result of retention on the polyacrylamide gel, retention on the G-25 resin during desalting steps (at least 1-2% of the total radioactivity) and loss during ethanol precipitation steps. However, additional experiments are required to quantitatively determine the amount of radioactivity that is incorporated into the stem-loop, indicating if the significant radioactivity recovery we see after the initial precipitation is a result of the recovery of unincorporated labelled dITP. If this is the case, efforts must be towards maximizing incorporation, such as significantly extending incubation times of the incorporation reaction, or even employing another enzyme in the incorporation reaction.

4.2 Substrate Optimization

The stem – loop substrates **1a** to **1g** contained centrally located adenine or hypoxanthine mismatches in the stem region. No excision of adenine (under conditions of saturating DNA, for multiple turnover) was observed when paired with guanine, cytosine, or adenine, suggesting that (in the context of the stem – loop substrate) mispairing of adenine in the stem, was not sufficient to encourage hydrolysis of the *N*-

glycoside bond. This lack of adenine excision was also observed for the adenine bulge substrate (substrate **1i**). This result suggests that inefficient adenine excision by AlkA under these conditions may not be a result of limited base flipping, but a consequence of the stability of the *N*-glycoside bond. Conversely, excision of hypoxanthine was observed when paired with thymine, guanine and adenine. The similar excision rates for these mismatches demonstrate that AlkA activity is independent of any preference towards the identity of the opposing base. Similar results were observed previously for double stranded substrates containing 1-N^6-ethenoadenine mismatches (*21*). Evidence for this lack of preference towards the opposing base is also reflected in the lack of protein interaction with the opposing base and minimal protein interaction with the undamaged strand (*21, 56*). No excision of hypoxanthine was observed when paired with cytosine. This absence of AlkA activity with the C : I mismatch relative to the other hypoxanthine mismatches may result from stable C : I base pairing. Hypoxanthine demonstrates hydrogen bonding properties similar to guanine, and therefore can form a stable base pair with cytosine. The hypoxanthine bulge (substrate **1h**) was shown to be excised by AlkA with the greatest efficiency of all substrates tested. This observation may be a consequence of two factors; the first being that the hypoxanthine molecule is already in an extrahelical position, therefore bypassing the barrier to base flipping, and the second being that the *N* – glycoside bond of inosine is less stable than that of adenine. This latter point is confirmed by the rates of nonenzymatic *N*-glycoside hydrolysis for adenine and hypoxanthine (paired with cytosine). The nonenzymatic hydrolysis of hypoxanthine is 7.5× faster than that of adenine (*21*). Interestingly, adenine excision was previously observed when paired with guanine, cytosine and adenine in the context of a 25 base pair

double-stranded substrate, under saturating AlkA conditions (*21*). In addition, hypoxanthine excision was also observed when paired with cytosine in the context of a 25 base pair double-stranded substrate under multiple turnover conditions. These observations suggest that the size and sequence context of a substrate may play a role in the efficiency of *N*-glycoside hydrolysis. Previous studies of AAG-catalyzed hydrolysis of hypoxanthine suggest that removal may be affected by the bases flanking the lesion (*57*). Hypoxanthine excision was more efficient when flanked by 5'T and 3'A as opposed to 5'G and 3'C, suggesting that local DNA sequence context can affect base stacking interactions and thus influence base flipping. Studies of AlkA from the archaebacterium *Archaeglobus fulgidus* suggest that hypoxanthine excision requires at least two bases 5' to the lesion and at least four bases on the 3' side of the lesion (*58*). Structural analysis of the *E. coli* protein indicates that AlkA makes contacts with 2 phosphate groups 5' to the damaged base and 3 phosphate groups 3' to the damaged base (*56*). The 26 base stem – loop substrate is approximately half the size of the double stranded substrate, and meets this requirement with 6 bases 3' to the extrahelical hypoxanthine. We initially postulated that the excision observed with the double stranded substrate (and not the stem-loop substrates) may result from the larger substrate being able to orient better in the large active site, facilitating protein interaction with the DNA. However, the similar rates of excision observed for the 26, 34, 46 and 56 base stem – loop substrates (Table 1), demonstrate that the 6 bases 3' to the hypoxanthine bulge was sufficient for DNA-protein interaction and subsequent $N-$glycoside hydrolysis.

4.3 The Effect of hAPE1

An abasic (AP) site intermediate is formed by *N*-glycoside hydrolysis. This intermediate is quite toxic to the cell and can lead to the formation of strand breaks, resulting in disruptions to DNA replication and transcription and encouraging base misincorporation (*59*). AP sites can also interact with topoisomerase I, leading to DNA damage and cell death. As well, AP site interactions with topoisomerase II are believed to have an effect on cell cycle check points and apoptosis (*59*). An AP site is more deleterious to the cell than the lesion from which it was formed. Thus its processing must be efficient to avoid the accumulation of these sites in DNA. Studies have shown that DNA glycosylases demonstrate tight binding to abasic sites, possibly until further processing can take place, thus limiting the catalytic turnover of the glycosylase (*60*). hAPE1 initiates the removal of this intermediate by cleaving the phosphodiester bond 5' to the AP site. hAPE1 has been shown to increase the activity of uracil DNA glycosylase (UDG) (*59*), thymidine DNA glycosylase (TDG) (*61*) , hOGG1 (*62*), and MutY (*55*). It has been postulated that this increase in glycosylase activity results from an increase in the rate of dissociation of the glycosylase from the AP site. This increase in dissociation glycosylase may result from a direct interaction between the AP endonuclease and DNA glycosylase or competition between the endonuclease and glycosylase for the AP site.

Interestingly, we observed that AlkA catalyzed excision of hypoxanthine was not stimulated in the presence of hAPE1 (Table 2). A similar result was also previously observed for AAG catalyzed excision of hypoxanthine and 1, N^6 – ethenoadenine (*63*). This observation suggests that these broad specificity enzymes may exhibit slow base

excision, thus limiting the formation of AP sites, such that the rate of formation of these sites does not exceed the rate at which they are processed (*63*).

4.4 [1'-3H KIE] Measurement

The [1'-^{3}H] KIE value measured here for the AlkA catalyzed excision of hypoxanthine resulted from the comparison of isotope ratios in residual substrate purified from 0% and partial reactions, and were subsequently corrected for the extent of reaction. The accuracy of the [1'-^{3}H] KIE value reported here, may be verified if a similar measurment is obtained from the comparision of isotope ratios in the products purified from 50% and 100% reactions. However, this method may not be the most efficient method for KIE analysis, as the AlkA-catalyzed excision of hypoxanthine was slow in comparison to previously reported rates (*21*).

The [1'-^{3}H] KIE is an α-secondary KIE value. The word "secondary" indicates that this position is not involved in any bond making or breaking during *N*-glycoside hydrolysis. However this position can provide information about the environment of the anomeric carbon at the transition state.

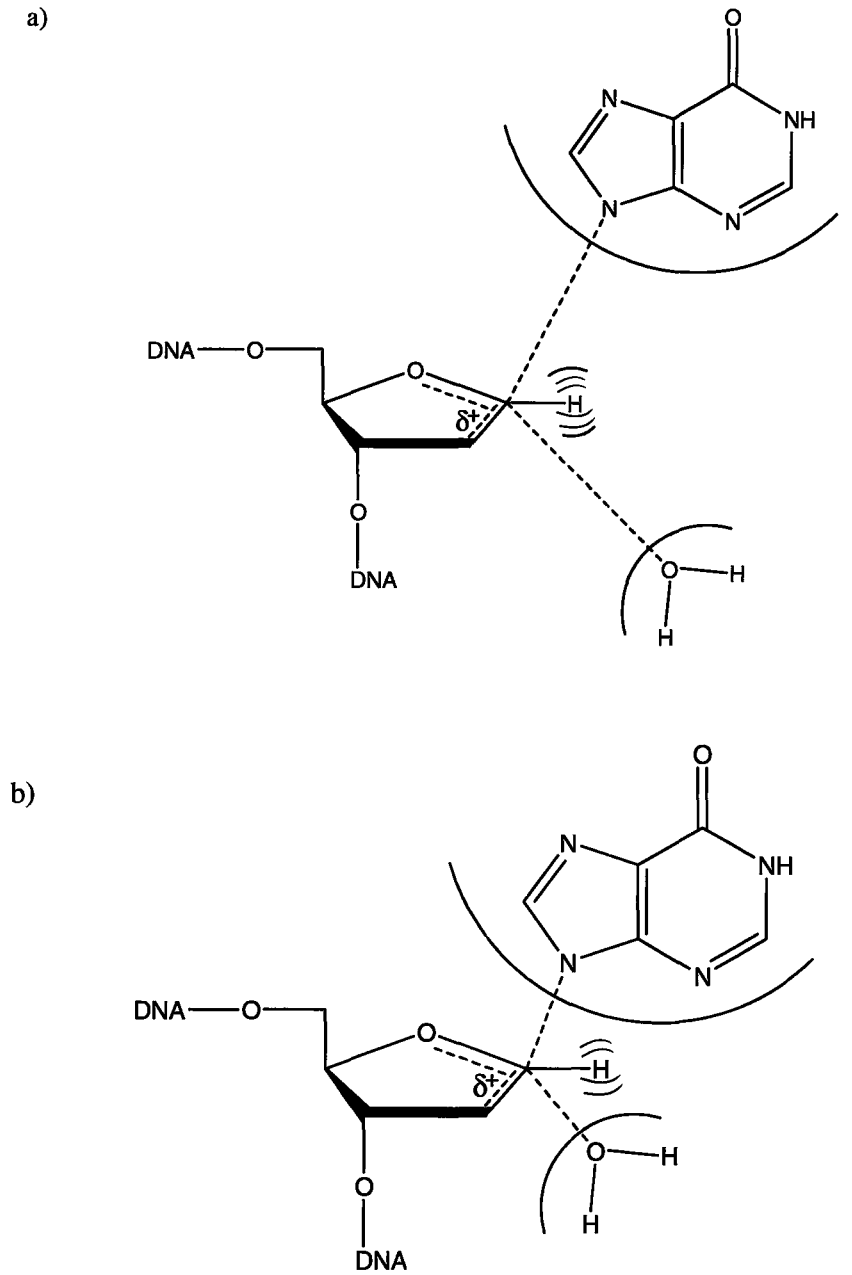

Figure 4.1. Vibrational freedom of H1'. (a) The vibrational freedom of H1' is greater in a dissociative S_N2 TS. (b) The proximity of the leaving group and nucleophile at the TS limits the vibrational freedom of H1' in an associative S_N2. Limited vibrational freedom of H1' has also been reported in early S_N1 TSs as well.

Typically large, normal [1'-^{3}H] KIE values have been associated with a dissociative reaction mechanism (a D_N*A_N or highly dissociative A_ND_N TS). These large values are a

reflection of the reduced steric crowding around the anomeric carbon. The re-hybridization of the anomeric carbon from sp^3 to sp^2 and the absence of the leaving group in a dissociative TS, results in an increase in the out-of-plane vibrational freedom of the H1' (Figure 4.1). Smaller or inverse [1'-^{3}H] KIE values have been commonly associated with a more synchronous A_ND_N TS. These smaller values are thought to be the result of increased steric crowding around the anomeric carbon, arising from the presence of both the nucleophile and leaving group at the TS. This increase in steric crowding limits the out-of-plane vibrational freedom of the H1' resulting in smaller [1'-^{3}H] KIE values. Typically the large, normal [1'-^{3}H] KIE values (>1.15) reported in the literature have been associated with either D_N*A_N or highly dissociative A_ND_N TSs, and the lone inverse value observed for thymine phosphorylase has been suggestive of a synchronous A_ND_N TS for this enzyme (*55*). However, it must be noted that a lack of precise correlation between experimentally observed [1'-^{3}H] KIE values and TS structures has limited any significant interpretation from these values.

The [1'-^{3}H KIE] value of 1.046 observed for AlkA-catalyzed *N*-glycoside hydrolysis while normal, was lower than [1'-^{3}H] KIE values observed for other DNA glycosylases. Interestingly, recent investigations into the transition state structures of 5'-methylthioadenosine nucleosidases (MTANs) reveals that these enzymes from *Neisseria meningitides* and *Helicobacter pylori* also exhibit small [1'-^{3}H] KIE values (*64, 65*). MTANs are members of the *N*-ribosyltransferase family of enzymes that catalyze the irreversible hydrolysis of 5'methylthioadenosine to 5' - methylthio – D – ribose and adenine, making the chemistry of these enzymes relevant to that of DNA glycosylases. MTANs are involved in purine and methionine salvage pathways, polyamine

biosynthesis, quorum sensing and methylation, and thus are promising antimicrobial targets (*64, 66, 67*). In humans, the MTAN is replaced by the 5'-methyladenosine phosphorylase (MTAP), an enzyme that catalyzes the reversible phosphorolysis of 5'-methylthioadenosine to 5'- methylthioribose-1-phosphate and adenine. This enzyme is currently being targeted for the design of anticancer agents (*64, 65, 68-70*) . The potential of these enzymes as antimicrobial and anticancer targets has resulted in extensive work towards solving the transition state structures and designing potent inhibitors. The majority of these enzymes demonstrate large [1'-^{3}H] KIE values, indicative of a highly dissociated TSs, with little bond order to the nucleophile and/or the leaving group adenine. However investigations into the TS structure of MTANs from *Neisseria meningitides* and *Helicobacter pylori* reveal [1'-^{3}H] KIE values of 1.030 ± 0.010 and 1.036 ± 0.004, respectively (*64, 65*). These small [1'-^{3}H] KIE values are suggestive of an early dissociative (D_N*A_N) TS, in which there is oxacarbenium ion character but also significant bond order to the leaving group adenine. It is postulated that this partial C1'-N9 bond sterically hinders the out-of-plane vibrational freedom of the H1', resulting in a smaller [1'-^{3}H] KIE. In addition to the MTANs of *Neisseria meningitides* and *Helicobacter pylori,* bovine purine nucleoside phosphorylase (bPNP), also demonstrates an early D_N*A_N TS. This is not seen in the TS structures of human and *Plasmodium falciparum* PNPs, which display highly dissociative S_N1 TSs. Interestingly human and bovine PNPs share 87% sequence identity and have completely conserved active sites, suggesting that even closely related enzymes can have different TS structures (*64, 65*). It must be noted that no extensive conclusions can be made regarding the single [1'-^{3}H] value reported here for AlkA. This measurement was a

proof-of-principle experiment, and the [1'-^{3}H] measurement must be repeated, additional KIEs measured, and commitment to catalysis examined in order to complete TS analysis of AlkA.

5.0 CONCLUSIONS AND FUTURE WORK

In the present study we have established that a stem-loop DNA structure is a substrate for AlkA. We have shown that the hypoxanthine bulge substrate is efficiently cleaved by the enzyme, and that this excision is exclusive to the bulge site. We have also shown that excision of the hypoxanthine bulge is more efficient than that of hypoxanthine mismatches, suggesting that use of this type of substrate avoids any barrier to base flipping. In contrast to previous studies, we observed no excision of adenine from the adenine bugle and adenine mismatch substrates; however, this may be a consequence of sequence context. In addition we have demonstrated that the presence of additional nucleotides (beyond the six of the 26 base stem-loop) down-stream of the bulge site did not improve excision, confirming that only a minimal number of contacts are made to the damaged strand.

We have developed an efficient method to synthesize labelled dITP for subsequent TS analysis, through modifications to the one-pot enzymatic synthesis of dATP used for MutY TS analysis. We were subsequently able to incorporate the labelled dITP into the 26 base stem-loop substrate.

A [1'-^{3}H] KIE measurement was performed using liquid scintillation counting. This measurement served as a proof-of-principle experiment, demonstrating that TS analysis of AlkA can be carried out using the hypoxanthine bulge substrate. While normal, the [1'-^{3}H] KIE value was small, suggestive of an early S_N1 (D_N*A_N) TS with oxacarbenium ion character but significant bond order to the leaving group base as well, or a relatively synchronous A_ND_N TS.

Future work is necessary to repeat the [1'-^{3}H] KIE measurement, ensuring reproducibility with this method and substrate. This will allow us to draw more extensive conclusions about the significance of the [1'-^{3}H] KIE value, and apply this method to KIE measurements at additional positions in the base and deoxyribose sugar. In addition, synthesis of the labelled stem-loop substrate needs to be optimized to improve overall radioactivity yields. Once a method for substrate synthesis and overall reproducibility of the KIE measurements is established, a complete TS analysis of AlkA can be performed. This information will provide insight into how this enzyme catalyzes *N*-glycoside hydrolysis for a variety of structurally diverse lesions.

REFERENCES

(1) Hollis, T., Ichikawa, Y., Ellenberger, T. (2000) DNA bending and a flip-out mechanism for base excision by the helix-hairpin-helix DNA glycosylase, Escherichia coli AlkA. *EMBO J. 19*, 758-766.

(2) Metz, A., Hollis, T., Eichman, B. . (2007) DNA damage recognition and repair by 3-methlyadenine DNA glycosylase I (TAG). *EMBO J. 26*, 2411-2420.

(3) Fortini, P. P., B., Parlanti, E., D'Errico, M., Simonelli, V., Dogliotti, E. (2003) The base excision repair: mechanisms and its relevance for cancer susceptibility. *Biochimie 85*, 1053-1071.

(4) Stivers, J. T., Jiang, Y.L. (2003) A mechanistic perspective on the chemistry of DNA repair glycosylases. . *Chem. Rev. 103*, 2729-2759.

(5) Tudek, B., Swoboda, M., Kowalczyk, P., Olinski, R. (2006) Modulation of oxidative DNA damage repair by the diet, inflammation and neoplastic transformation. *J. Physiol. Pharmacol. 57*, 33-49.

(6) Tsuzuki T, Y., N., Nakabeppu, Y. (2007) Significance of error-avoiding mechanisms for oxidative damage in carcinogenesis. *Cancer Science 95*, 465-470.

(7) Sedgwick, B. (2004) Repairing DNA methlyation damage. *Nature Reviews 5*, 148-157.

(8) Tudek, B., VanZeeland, A.A., Kusmierek, J.T., Laval, J. (1998) Activity of *Escherichia coli* DNA glycosylases on DNA damaged by methylating and ethylating agents and influence of 3-substitued adenine dervivatives. *Mutat. Res. 407*, 169-176.

(9) Budke, B., Kuzminov . . (2006) Hypoxanthine incorporation is nonmutagenic in *Escherichia coli. J. Bacteriol. 188*, 6553-6560.

(10) Terato, H., et al. (2002) Novel repair activities of AlkA and endonuclease VIII for xanine, and oxanine, guanine lesions induced by nitric oxide and nitrous acid. *Nucleic Acid Res. 30*, 4975-4984.

(11) Yao, M., Kow, Y.W. (1995) Interaction of deoxyinosine 3'-endonuclease from *Escherichia coli* with DNA containing deoxyinosine. . *J. Biol. Chem. 270*, 28609-28616.

(12) Nordmann, P. L., Markis, C., Reznikoff, W.S. . (1988) Inosine induced mutations. *Mol. Gen. Genet. 214*, 62-67.

(13) Wink, D. A., et al. (1998) The multifaceted roles of nitric oxide in cancer. *Carcinogenesis 19*, 711-721.

(14) Ohshima, H. B., et al. . (1994) Chronic infections and inflammatory processes as cancer risk factors: possible role of nitric oxide in cancer. *Mutat. Res. 305*, 253-264.

(15) Weissman, L., Jo, D.G., Sorensen, M.M., Souza-Pinto, N.C., Markesbery, W.R., Mattson, M.P., Bohr, V.A. (2007) Defective DNA base excision repair in brain from individuals with Alzheimer's disease and amnestic mild cognitive impairment. *Nucleic Acid Res. 35*, 5545-5555.

(16) Mishina, Y., Duguid, E., He, C. (2006) Direct reversal of DNA alkylation damage. *Chem. Rev. 106*, 215-232.

(17) Felton, K., Gilchrist, D., Andrew, S. . (2007) Constitutive deficiency in DNA mismatch repair. *Clin. Genet. 71*, 483-498.
(18) Baker, e. a. (2007) Nucleotide excision repair eliminates unique DNA-protein cross-links from mammalian cells. *J. Biol. Chem. 282*, 22592-22604.
(19) Reardon, J. T., Sancar, A. . (2003) Recognition and repair of cyclobutane thymine dimer, a major cause of skin cancers, by the human excision nuclease. *Genes and Development 17*, 2539-2551.
(20) Bailly, V., Verly, W.G. (1988) Possible roles of beta-elimination and gamma elimination reactions in the repair of DNA containing AP sites in mammalian cells. *Biochem. J. 253*, 533-559.
(21) O'Brien, P. J. E., T. (2004) The *Escherichia coli* 3-methyladenine DNA glcosylase AlkA has a remarkably versatile active site. *J. Biol. Chem. 279*, 26876-26884.
(22) Berti, P. J., McCann, J.A.B.. (2006) Toward a detailed understanding of base excision repair enzymes: Transition state and mechanistic analyses of *N*-Glycoside hydrolysis and *N*-glycoside transfer. *Chem. Rev. 106*, 506-555.
(23) Berdal, K. G., Johansen, R.F., Seeberg, E. . (1998) Release of normal bases from intact DNA by a native DNA repair enzyme. *EMBO J. 17*, 363-367.
(24) Guthrie, R. D., Jencks, W. P. , . (1989) IUPAC recommendations for the representation of reaction mechanisms. *Acc. Chem. Res. 22*, 343-349.
(25) Becker, e. a. (1998) MutY catalytic core, mutant and bound adenine structures define specificity for DNA repair enzyme superfamily. *Nature Structural Biology 5*, 1058-1064.
(26) Denver, D. R., Swenson, S.L., Lynch, M. (2003) An evolutionary analysis of the helix-hairpin-helix superfamily of DNA repair glycosylases. *Mol. Biol. Evol. 20*, 1603-1611.
(27) Doherty, A. J., Serpell, L.C., Ponting, C.P. . (1996) The helix-hairpin-helix DNA binding motif: a structural basis for non-sequence-specific recognition of DNA. *Nucleic Acid Res. 24*, 2488-2497.
(28) Ramstein, J. (1988) Energetic coupling between DNA bending and base pair opening. *Proc. Natl. Acad. Sci. U.S.A. 85*, 7231-7235.
(29) Fuxreiter, M., Luo, N., Jedlovszky, P., Simon, I., Osman, R. (2002) Role of base flipping in specific recognition of damaged DNA by repair enzymes. *J. Mol. Biol. 323*, 823-834.
(30) Yang, W. (2006) Poor base stacking at DNA lesions may initiate recognition by many repair proteins. *DNA Repair*.
(31) Bloom, B. L., et al. . (2005) The efficiency of hypoxanthine excision by alkyladenine DNA glycosylase is altered by changes in nearest neighbour bases. *DNA Repair 4*, 1088-1098.
(32) Pankiewicz, K. W., Watanabe, K.A. . (1999) Kinetic mechanism of damage site recognition and uracil flipping by *Escherichia coli* and uracil DNA glycosylase. *Biochemistry 38*.
(33) Parikh, S. S., et al. . (1998) Base Excision repair initiation revealed by crystal structures and binding kinetics of human uracil-DNA glycosylase with DNA. *EMBO J. 17*, 52214-52216.

(34) Mol, C. D., Arvai, A.S., Begley, T.J., Cunningham, R.P., Tainer, J.A. . (2002) Structure and activity of a thermostable thymine DNA glycosylase evidence for base twisting to remove mismatched normal DNA bases. *J. Mol. Biol. 315*, 373-384.

(35) Fromme, J. C. B., A; Huang, S.J; Verdine, G.L. (2004) Structural basis for removal of adenine mispaired with 8-oxoguanine by MutY adenine DNA glycosylase. *Nature 427*, 652-656.

(36) Norman, D. P. G. C., S.J; Verdine, G.L. (2003) Structural and biochemical exploration of a critical amino acid in human 8-oxoguanine glycosylase. *Biochemistry 42*, 1564-1572.

(37) Lindahl, T., Sedgwick, B., Seikiguchi, M., Nakabeppu, Y. . (1988) Regulation and expression of the adaptive response to alkylating agents. *Annu. Rev. 57*, 133-157.

(38) Labahn, J., Scharer, O.D., Long, A., Ezaz-Nikpay, K., Verdine, G.L. . (1996) Structural basis for the exicison repair of alkylation-damaged DNA. *Cell 86*, 321-329.

(39) Yamagata, Y., et al. (1996) Three-dimesonal structure of a DNA repair enzyme, 3-methyladenine DNA glycosylase II, from *Escherichia coli. Cell 86*, 311-319.

(40) O'Brien, P. J., Ellenberger, T. (2003) Human alkyladenine DNA glycosylase uses acid-base catalysis for selective excision of damaged purines. *Biochemistry 43*, 12418-12429.

(41) Lau, A., et al. . (1998) Crystal structure of a human alkylbase-DNA repair enzyme complexed to DNA: Mechanisms for nucleotide flipping and base excision. *Cell 95*, 249-258.

(42) Ellenberger, T., et al. (2000) Molecular basis for discriminating between normal and damaged bases by the human alkyladenine glycosylase, AAG. *Proc. Natl. Acad. Sci. U.S.A. 97*, 13573-13578.

(43) Shi, W., Schramm, V.L., Almo, S.C. . (1999) Nucleoside hydrolase from *Leishmania major. J. Biol. Chem. 30*, 21114-21120.

(44) Deganno, M., Almo, S.C., Sacchettini, J.C., Schramm, V.L. (1998) Trypanosomal nucleoside hydrolase. A novel mechanism from the structure with a transition state inhibitor. *Biochemistry 37*, 6277-6285.

(45) Versees, W., Decanniere, K., Van Holsbeke, E., Devroede, N., Steyaert, J. (2002) Enzyme-substrate interactions in the purine-specific nucleoside hydrolyase from *Tyrpanosoma vivax. J. Biol. Chem. 277*, 15938-15946.

(46) Lee, J., Cornell, K. A., Riscoe, M.K., Howell, P.L. . (2003) Structure of *Escherichia coli* 5 -methylthioadenosine/S-adenosylhomocysteine nucleosidase inhibitor complexes provide insight into the conformational change required for substrate binding and catalysis. *J. Biol. Chem. 278*, 8761-8770.

(47) Versees, W., Loverix, S., Vandelmeulebrouke, A., Geerlings, P., Steyaert, J. (2004) Leaving group activation by aromatic stacking: An alternative to general acid catalysis. *J. Mol. Biol. 338*, 1-6.

(48) Huskey, W. P. (1991) Enzyme Mechanism from Isotope Effects, (Cook, P. F., Ed.) pp 37-72, CRC Press Inc.

(49) Berti, P. J., Schramm, V.L. (1997) Transition state structure of the solvolytic hydrolysis of NAD+. *J. Am. Chem. Soc. 119*, 12069-12078.

(50) Parkin, D. W. (1991) Enzyme Mechanism from Isotope Effects, (Cook, P. F., Ed.) pp 269-290, CRC Press Inc.
(51) Laemmli, U. K. (1970) Cleavage of structural proteins during the assembly of the head of Bacteriophage T4. *Nature 227*, 680-685.
(52) Werner, R. M., Stivers, J.T. (2000) Kinetic isotope effect studies of the reaction catalyzed by uracil DNA glycosylase: Evidence for an oxocarbenium ion-uracil anion Intermediate. *Biochemistry 39*, 14054-14064.
(53) Parkin, D. W., Leung, H.B., Shcramm, V.L. (1984) Synthesis of nucleotides with specific radiolabels in ribose. Primary ^{14}C and secondary ^{3}H kinetic isotope effects on acid-catalyzed glycosidic bond hydrolysis of AMP, dAMP, and inosine. *J. Biol. Chem. 259*, 9411-9417.
(54) McCann, J. A. B. (2006) in *Biochemistry and Biomedical Sciences*, McMaster University, Hamilton.
(55) McCann, J. A. B. (2006) in *Biochemistry and Biomedical Sciences*, McMaster University, Hamilton.
(56) Stivers, J. T. J., Y.L. (2003) A mechanistic perspective on the chemistry of DNA repair glycosylases. *Chem. Rev. 103*, 2729-2759.
(57) Vallur, A. C. M., R.L.; Bloom, L.B. (2005) The efficiency of hypoxanthine on excision by alkyladenine DNA glycosylase is altered by changes in nearest neighbour bases. *DNA Repair 4*, 1088-1098.
(58) Mansfield, C. K., S.M.; McCarthy, T.V. (2003) Characterization of *Archaeglobus fulgidus* AlkA hypoxanthine DNA glycosylase activity. *FEBS J. 540*, 171-175.
(59) Parikh, S. S. e. a. (1998) Base excision repair initiation revealed by crystal structures and binding kinetics of human uracil-DNA glycosylase with DNA. *EMBO J. 17*, 5214-5226.
(60) Scharer, O. D. e. a. (1998) Specific binding of a designed pyrrolidine abasic site analog to multiple DNA glycosylases. *J. Biol. Chem. 273*, 8592-8597.
(61) Waters, T. R. G., P; Jiricny, J; Swann, P.F. (1999) Human thymine DNA glycosylase binds to apurinic sites in DNA but is displaced by human apurinic endonuclease I. *J. Biol. Chem. 274*, 67-74.
(62) Vidal, A. E. H., I.D; Boiteux, S; Radicella, J.P. (2001) Mechanism of stimulation of the DNA glycosylase activity of hOGG1 by the major AP endonuclease: bypass of the AP lyase activity step. *Nucleic Acid Res. 29*, 1285-1292.
(63) Maher, R. L. e. a. (2006) Slow base excision by human alkyladenine DNA glycosylase limits the rate of formation of AP sites and AP endonuclease 1 does not stimulate base excision. *DNA Repair*.
(64) Singh, V. L., M.; Brown, R.L.; Norris, G.E.; Schramm, V.L. (2007) Transition state structure of *Neisseria meningitides* 5'-methylthioadenosine/*S*-adenosylhomocysteine nucleosidase. *J. Am. Chem. Soc. 129*, 13831-13833.
(65) Gutierrez, J. A. L., M.; Singh, V.; Li, L.; Brown, R.L.; Norris, G.E.; Evans, G.B.; Furneaux, R.H.; Tyler, P.C.; Painter, G.F.; Lenz, D.H.; Schramm, V.L. (2007) Picomolar inhibitors as transition state probes of 5'-methyladenosine nucleosidases. *ACS Chemical Biology 2*, 725-733.
(66) Singh, V. L., J.E.; Nunez, S.; Howell, P.L.; Schramm, V.L. (2005) Transition state structure of 5'methylthioadenosine/S-adenosylhomocysteine nucleosidase

. from *Escherichia coli* and its similarity to transition state analogues. *Biochemistry 44*, 11649-11659.

(67) Singh, V. E., G.B.; Lenz, D.H.; Mason, J.M.; Clinch, K.; Mee, S.; Painter, G.F.; Tyler, P.C.; Furneaux, R.H.; Lee, J.E.; Howell, L.P.; Schramm, V.L. (2005) Femtomolar transition state analogue inhibitors of 5'-methylthioadenosine/S-adenosylhomocysteine nucleosidase from *Escherichia coli. J. Biol. Chem. 280*, 18265-18273.

(68) Singh, V. S., V.L. (2007) Transition state analysis of *S.pneumoniae* 5'-methylthioadenosine nucleosidase. *J. Am. Chem. Soc. 129*, 2783-2795.

(69) Singh, V. S., V.L. (2006) Transition state structure of human 5'-methylthioadenosine phosphorylase. *J. Am. Chem. Soc. 128*, 14691-14696.

(70) Evans, G. B. F., R.H.; Lenz, D.H.; Painter, G.F.; Schramm, V.L.; Singh, V.; Tyler, P.C. (2005) Second generation transition state analogue inhibitors of human 5'-methylthioadenosine phosphorylase. *J. Med. Chem. 48*, 4679-4689.